Modeling slow slip events and megathrust earthquakes in the Costa Rica subduction zone

Author: Lise Alalouf, Earth and Planetary Sciences, McGill University, Montréal

Supervisor: Yajing Liu, Earth and Planetary Sciences, McGill University, Montréal

A thesis submitted in partial fulfilment for the requirement of the degree of Master of Science

Acknowledgements

First and foremost, I would like to thank my supervisor, Yajing Liu, for her trust, time and regular reviews throughout my thesis project. I would also like to thank my friends and colleagues with whom I shared my office: Andres Pena Castro, Julia Morales-Aguirre, John Onwuemeka, Ge Li, Brindley Smith, Alessandro Verdecchia, Ruhollah Keshvardoost, Clément Estève and Julia Kubanek for the good times we shared, their support and many advices. I would also like to thank my modeling companions who, despite the distance, helped me throughout my project, with kind and helpful emails: Hongyu Yu, Lei Zhang and Duo Li. I would also like to thank my ”German” collegues for the regular discussions and meetings: Rebecca Harrington, Gian Maria Bocchini, Kilian Kemna, Marco Roth, Ricarda Wache, and Gianina Meneses. Finally, I would like to thank my committe members for their follow-up and advices : Yajing Liu, Fiona Darbyshire, Rebecca Harrington, Jamie Kirkpatrick and Bill Minarik. On a more personal note, I would like to thank my other McGill friends who were a few offices away from me, especially Pascale Daoust, without whom my life at McGill would not have been the same. I would like to thank my parents, Annick et Denis Alalouf, for their unending support in finishing my thesis, my sister and her husband, Diane Alalouf-Hall and Vincent Hall, for welcoming me into their home and guiding me through Montreal life. Finally, I would like to thank my husband, Romain Schmitt, for always being my support, for having always been there to accompany me and believe in me.

Abstract

Subduction zones are where the largest earthquakes occur. In recent decades, scientists have also discovered the presence of episodic aseismic slip, including slow slip events (SSE), along most of the subduction zones. However, it is still unclear how these SSEs can influence megathrust ruptures. The Costa Rica subduction zone is a particularly interesting area as a SSE was recorded 6 months before the 2012 Mw7.6 earthquake, in the Nicoya Peninsula, suggesting potential stress transfer from the SSE to the earthquake slip zone. SSEs beneath the Nicoya Peninsula have also been recorded both updip and downdip of the seismogenic zone, making it a unique area to study the complex interaction between SSEs and earthquakes. We conducted an initial study, using GPS inversion from previous studies, to observe the empirical relationships of various source parameters between SSEs and megathrust earthquakes along the Costa Rica subduction zone. These scaling relationships highlight the differences and similarities between SSEs and megathrust earthquakes and and allows to better explain the physical mechanisms at the base of the SSEs. It was observed that static stress drop of earthquakes and the static stress drop of SSEs do not follow the same trend. Indeed, even if the stress drops remains constant for different sized event, they are 1-2 orders of magnitude lower for SSEs than for earthquakes, which agrees with stress drop analyses performed in other subduction zones. We also found that the duration-moment scale for SSEs of Costa Rica is $M_0 \propto T$, where M_0 is the equivalent moment and T is the event duration. Then, to better understand how updip and downdip SSEs and megathrust earthquakes may be related, we performed a numerical simulation study. As

most of the SSEs (shallow and deep) were recorded around the Nicoya Peninsula, we decided to use a 1D linear fault integrated in a homogeneous elastic half-space, with different dip angles along several geometric profiles of the subduction fault under the Nicoya Peninsula of the Costa Rica margin. This 1D modelling in the framework of the rate-and-state friction law, allows us to study the interaction between SSEs and megathrust ruptures with high numerical resolution and relatively short computation times. The model provides information on the long-term seismic history by reproducing the different stages of the seismic cycle (interseismic slip, shallow and deep episodic slow slip, and coseismic slip). We investigated the influence of the variation of numerical parameters and frictional properties on the recurrence interval, maximum slip velocity and cumulative slip of SSEs (both shallow and deep) and earthquakes, and their interaction. For an assumed friction parameters, $a - b$ profile, that we defined from thermal evolution of the Costa Rica subduction zone, we varied effective normal stress and characteristic slip distance until the model replicated the observed recurrence intervals for SSEs ($\sim$ 20-22 months) and earthquakes ($\sim$ 50 years) under the Nicoya Peninsula. Then, we compared our results with GPS and seismic observations (i.e. cumulative slip, characteristic duration, moment rate, rupture depth and size) to identify an optimal set of model parameters to understand the interaction between different modes of subduction fault deformation. We defined the optimal set of parameters as L = 0.2 - 0.8 mm and $\bar{\sigma}$ = 0.4 - 2.4 MPa for SSEs and L = 10 mm and $\bar{\sigma}$ = 35 MPa for earthquakes.

Our results show that parameters such as characteristic slip distance and effective normal stress strongly impact on the long-term history fault slip of Costa Rica, both on the recurrence interval between SSEs and on the SSE maximum slip velocity, which is consistent with previous numerical studies. We also found through simulation that updip and downdip SSEs do not behave in the same way for the same set of parameters. Deep SSEs have shorter recurrence intervals and higher maximum slip rates but shorter durations than shallow SSEs. In addition, we observe a deep loading phase prior to the earthquake rupture where, in the few years prior to the earthquake, SSEs occur more frequently and the maximum slip rate is higher, which could represent a distinctive earthquake preparation phase. While for shallow SSEs, the loading prior to an earthquake rupture is represented by more temporally spaced SSEs, with higher maximum slip rates.

Résumé

Les zones de subduction sont les endroits où se produisent les plus grands séismes. Au cours des dernières décennies, les scientifiques ont également découvert la présence de glissements asismiques épisodiques, y compris des glissements lents (SSE), le long de la plupart des zones de subduction. Cependant, on ne sait toujours pas comment ces glissements lents peuvent influencer les ruptures de mégaséismes. La zone de subduction du Costa Rica est une zone particulièrement intéressante car un SSE a été enregistré 6 mois avant le séisme Mw7.6 de 2012, dans la péninsule de Nicoya, ce qui suggère un transfert potentiel de contraintes de l'ESS vers la zone de glissement du séisme. Les SSE sous la péninsule de Nicoya ont également été enregistrés en amont et en aval de la zone sismogénique, ce qui en fait une zone unique pour étudier l'interaction complexe entre les SSE et les séismes. Nous avons mené une première étude, en utilisant des inversions GPS d'études précédentes, pour observer les relations empiriques de divers paramètres à la source entre les SSE et les mégaséismes le long de la zone de subduction du Costa Rica. Ces relations d'échelle mettent en évidence les différences et les similitudes entre les SSE et les mégaséismes et permettent de mieux expliquer les mécanismes physiques à la base des SSE. Il a été observé que la chute de contrainte statique des séismes et la chute de contrainte statique des SSE ne suivent pas la même tendance. En effet, même si les chutes de contraintes restent constantes pour des événements de tailles différentes, elles sont de 1 à 2 ordres de grandeur plus faibles pour les SSE que pour les séismes, ce qui est en accord avec les analyses de chutes de contraintes réalisées dans d'autres zones de subduction. Nous avons

également constaté que l'échelle durée-moment pour les SSE du Costa Rica est $M_0 \propto T$, où M_0 est le moment équivalent et T est la durée de l'événement. Ensuite, pour mieux comprendre comment les SSE en amont et en aval et les mégaséismes peuvent être liés, nous avons réalisé une étude de simulation numérique. Comme la plupart des SSE (superficiels et profonds) ont été enregistrés autour de la péninsule de Nicoya, nous avons décidé d'utiliser une faille linéaire 1D intégrée dans un demi-espace élastique homogène, avec différents angles de pendage le long de plusieurs profils géométriques de la faille de subduction sous la péninsule de Nicoya de la marge du Costa Rica. Cette modélisation 1D dans le cadre de la loi de friction taux-état, nous permet d'étudier l'interaction entre les SSE et les mégaruptures avec une haute résolution numérique et des temps de calcul relativement courts. Le modèle fournit des informations sur l'histoire sismique à long terme en reproduisant les différentes étapes du cycle sismique (glissement intersismique, glissement lent épisodique peu profond et profond, et glissement cosismique). Nous avons étudié l'influence de la variation des paramètres numériques et des propriétés de friction sur l'intervalle de récurrence, la vitesse maximale de glissement et le glissement cumulé des SSE (à la fois superficiels et profonds) et des séismes, ainsi que sur leur interaction. Pour un paramètre de friction supposé, le profil $a - b$, que nous avons défini à partir de l'évolution thermique de la zone de subduction du Costa Rica, nous avons fait varier la contrainte normale effective et la distance de glissement caractéristique jusqu'à ce que le modèle reproduise les intervalles de récurrence observés pour les SSE ($\sim$ 20-22 mois) et les séismes ($\sim$ 50 ans) sous la péninsule de Nicoya. Ensuite, nous avons comparé nos résultats avec les observations GPS et sismiques (c'est-à-dire le glissement cumulé, la durée caractéristique, le taux de moment, la profondeur et la taille de la rupture) afin d'identifier un ensemble optimal de paramètres du modèle pour comprendre l'interaction entre les différents modes de déformation des failles de subduction. Nous avons défini l'ensemble optimal de paramètres comme étant L = 0,2 - 0,8 mm et $\bar{\sigma}$ = 0,4 - 2,4 MPa pour les SSE et L = 10 mm et $\bar{\sigma}$ = 35 MPa pour les séismes.

résultats montrent que des paramètres tels que la distance caractéristique de glissement et la contrainte normale effective ont un impact important sur le glissement de la faille à long terme du Costa Rica, à la fois sur l'intervalle de récurrence entre les SSE et sur la vitesse maximale de glissement des SSE, ce qui est cohérent avec les études numériques précédentes. Nous avons également constaté par simulation que les SSE en amont et en aval ne se comportent pas de la même manière pour le même ensemble de paramètres. Les SSE profonds ont des intervalles de récurrence plus courts et des taux de glissement maximum plus élevés mais des durées plus courtes que les SSE superficiels. En outre, nous observons une phase de charge profonde avant la rupture du séisme où, dans les quelques années précédant le séisme, les SSE se produisent plus fréquemment et le taux de glissement maximal est plus élevé, ce qui pourrait représenter une phase distincte de préparation au séisme. Alors que pour les SSE superficiels, le chargement avant la rupture d'un séisme est représenté par des SSE plus espacées dans le temps, avec des taux de glissement maximum plus élevés.

Contents

List of Figures

List of Tables

1 Introduction

Earthquakes along subduction zones have been long studied because they are the largest in magnitude and often very damaging to coastal areas. However, the mechanism of megathrust earthquakes is still not well understood, particularly since the discovery of slow slip events (SSEs) (e.g. Dragert et al. (2001)), showing that fast ruptures at subduction zone are not the only type of deformation along plate interfaces. SSEs, similar to regular earthquakes in that they are caused by shear rupture and slip on or near the plate interface, host a fraction of the cumulative slip on plate boundary faults. However, these events have significantly slower rupture velocities (duration from days to years) and are too slow to radiate seismic energy. Slow slip events can release elastic energy equivalent to moment magnitude (Mw) 6.0 or higher spread over a long period. Even if the typical recurrence interval (from months to years) of slow earthquakes is much shorter than those of megathrust earthquakes, the repetitive nature of slow earthquakes may be a useful tool for improving our understanding of rupture styles and the recurrence cycle of megathrusts (Obara & Kato 2016). Slow slip events have been registered in many subduction zone, however, they were mostly recorded in the transition zone below the seismogenic zone. SSEs are located at the unstable-stable transition zone under the generic rate-state framework, i.e. without other mechanisms like dilatancy, both updip and downdip the seismogenic zone. We call them shallow SSEs for the SSEs located in the updip transition zone, and deep, for the SSEs located in the downdip transition zone. Only a few areas have recorded SSEs in the upper zone of the seismogenic zones (i.e. Japan, Costa Rica, New Zealand).

1.1 Current Understanding of SSEs

The discovery of SSEs is quite recent, and sheds light on the researches of megathrust ruptures. SSEs were first discovered, relatively simultaneously, both near the Bungo Channel (Hirose et al. 1999) and in the Cascadia subduction zone (Dragert et al. 2001) but were then localized in numerous subduction zones (Ito et al. 2013, Socquet et al. 2017) and even in other tectonic settings such as the transform fault of San Andreas (Linde et al. 1996, Rousset et al. 2019) and beneath the Kilauea volcano in Hawaii (Segall et al. 2006). Hawaii SSEs occured at shallow depths (around 10 km depth), with low temperature and pressure allowing aseismic fault slip on velocity-strengthening fault zones without the need for high pore fluid pressures (Marone et al. 1991), while tremors where detected in San Andreas at depth ranging from 18 to 28 km, probably related to variations in frictional properties and fluid pressures (Shelly & Hardebeck 2010). Slow slip events (SSEs) represent a distinct strain release process that occurs in many subduction zones (Dragert et al. 2001, Obara et al. 2004, Outerbridge et al. 2010), that are characterized by slow rupture speeds, so slow that they do not radiate any detectable signals. Therefore, the most reliable way to record and document them is by using continuous geodetic observations. The complete mechanisms of SSEs are not fully understood. Some studies suggest that SSEs have similar mechanisms to ordinary earthquakes and are thought to be caused by slip on faults. SSEs are inferred with low stress drop, on the order of a few kPa (Rubinstein et al. 2007). In subduction areas they can occur updip and downdip of seismogenic zone, even if in most cases they have only been registered downdip, near or within low-velocity layer characterized by high velocity ratio value, commonly interpreted as near lithostatic pore-fluid pressure (Audet & Schaeffer 2018). On average SSEs have slip rates of 10-100 times higher than plate convergences and last for days to months (Dragert et al. 2001, Schwartz & DeShon 2007). Even if they have low slip rates, they can still release elastic energy equivalent to Mw 6.0 earthquakes. From modeling studies, it seems that almost all SSEs are inferred to appear around the frictional transition portion from unstable to stable fault slip (Schwartz & DeShon 2007, Ishida et al. 2013, Kano et al. 2018).

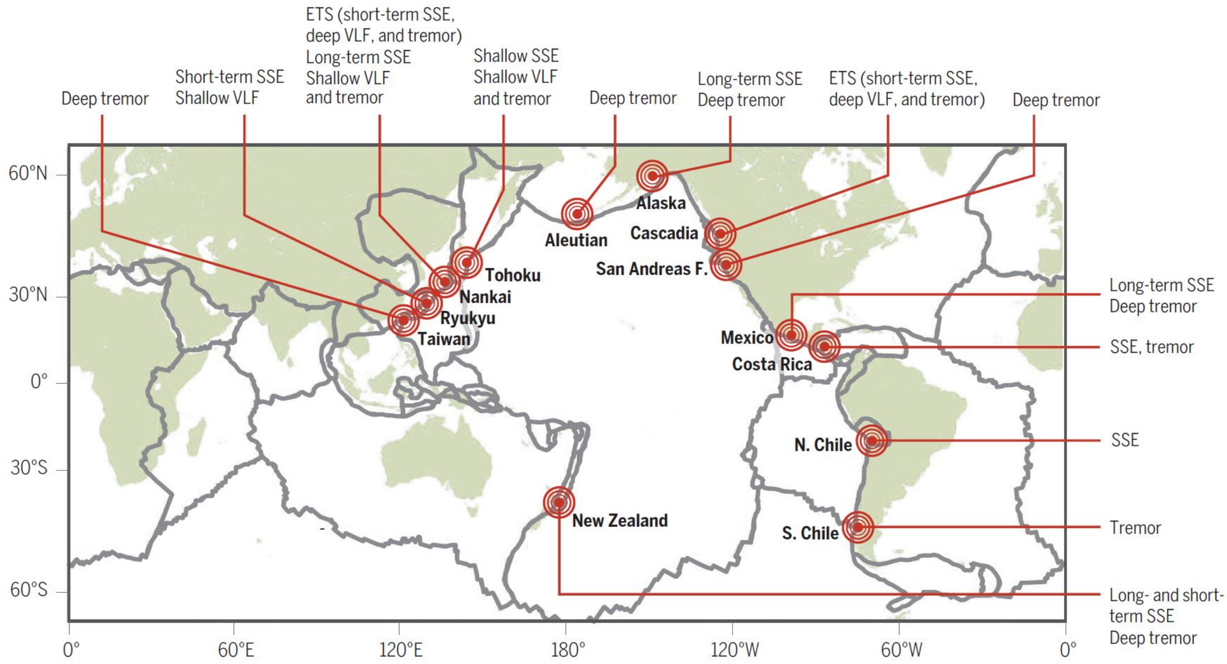

Figure 1.1: Global distribution of slow earthquakes: VLF (very low frequency events), SSE (slow slip event), tremor (seismic signal of slow earthquakes) and ETS (episodic tremor and slip). From Obara & Kato (2016).

Based on the observations, the occurrence of SSEs is closely related with the existence of high pore fluid near the subduction fault (Obara 2002, Rogers & Dragert 2003). From Obara (2002) study, it is hypothesized that the near-lithostathic pore fluid reduces the normal stress loading on the fault and promotes the fault shear slip. The importance of the high fluid pressure in generating slow earthquakes is supported by several observed pieces of evidence. The recurrence of SSEs is modulated by small stress perturbations of a few kPa, such as tidal stressing (Hawthorne & Rubin 2013) or passing-by surface waves (Rubinstein et al. 2007, Peng et al. 2009). The sensitivity to small stress perturbations suggests the fault is critically stressed.

Shallow and deep slow slip events occur at areas with large differences in temperature and pressure, but in both case seems to be related to changes in pore-fluid pressure related to dehydration reactions (Outerbridge et al. 2010, Voss et al. 2017). However, recent studies showed that shallow and deep they are not acting the same on the interseismic locking, with deep SSEs releasing most of the locking while shallow SSEs only account for a portion of the interseismic locking (Dixon et al. 2014), which leads to questions about physical processes that may be responsible for these differences. Understanding slow earthquakes should lead to new insights into the physics of plate subduction and in assessing the probability of future large earthquakes.

1.2 Relation with Megathrust Earthquakes

The influence of SSEs on megathrust earthquakes is currently not well understood. In some cases, SSEs precede subduction zone earthquakes indicating possible triggering by stress transfer by causing stress perturbations on adjacent fault segments (e.g. 2011 M_W 9.0 in Japan, 2014 M_W 8.1 in Chile, 2018 M_W 6.9 in Greece), sometimes triggering devastating earthquakes (Obara & Kato 2016, Uchida et al. 2016, Socquet et al. 2017, Mouslopoulou et al. 2020). Numerical simulations also proposed that SSEs could evolve into megathrust earthquakes (Segall & Bradley 2012), even if no evidence has been observed so far. While in other cases, SSEs may reduce the probability of large earthquakes by relieving strain during the inter-seismic period, and reducing the magnitude of the megathrust rupture as well as tsunami potential (Voss et al. 2018, Dixon et al. 2014, Rolandone et al. 2018). Recent modeling works have revealed intriguing changes of SSE behavior before and after earthquake (Luo & Liu 2019), where the recurrence intervals and maximum slip rates show an important decrease right before the megathrust rupture. Change in the SSE reccurence interval have been observed from GPS inversion in some areas such as the Bungo Channel in Japan (Ozawa 2014) and the Mexico subduction zone (Graham et al. 2015).

It shows that precisely measuring and characterizing SSEs may help to define future earthquake rupture time and area, as well as better understanding the physical conditions on the seismogenic plate interface.

1.3 The Costa Rica Subduction Zone

The Costa Rica subduction zone is an oblique subduction where the Cocos plate is subducting beneath the Caribbean plate at a convergence rate of 8-9 cm/yr (DeMets 2001) along the Middle American Trench. In Costa Rica, earthquakes with magnitudes greater than 7 occur

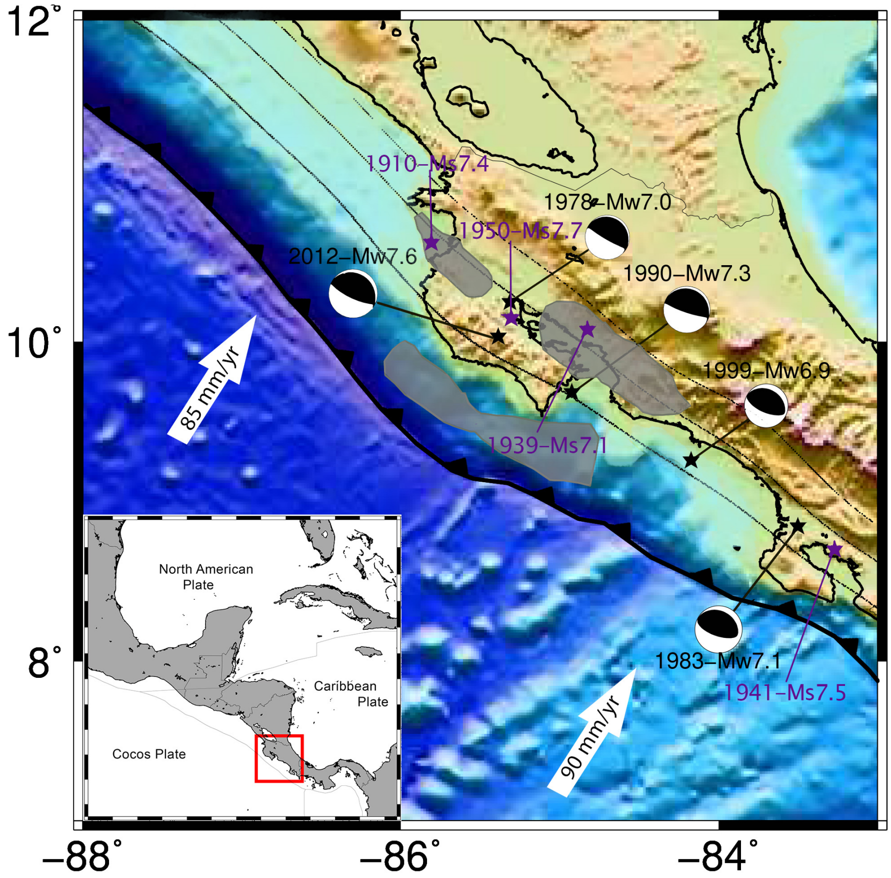

Figure 1.2: Large events occurring at Costa Rica. Focal mechanisms from GCMT catalog. Shaded areas summed SSE slip for the entire 1950-2012 period (Dixon et al. 2014). Texts in purple are the historical earthquakes (Protti et al. 1994)(and references therein). Dashed lines are slab contour every 20 km.

approximately every 50-60 years. In 2002, a network of continuous GNSS stations was initiated and allowed to record both the late and eartly stages of earthquake cycles, with several critical processes, such as inter-seismic coupling (Feng et al. 2012), coseismic rupture (Yue et al. 2013), postseismic behavior (Hobbs et al. 2017), and SSEs (Jiang et al. 2012, Voss et al. 2017). Also, numerous SSEs have been recorded both updip and downdip of the seismogenic zone (i.e. Table1.1), particularly a SSE has been recorded in the six months preceding the 2012 Mw 7.6 earthquake (Voss et al. 2018). More recently the 2017 Mw 6.5 was recorded near an identified SSE (Xie et al. 2020), suggesting potential stress transfer between SSE and megathrust rupture (Liu & Rice 2007). SSEs in Costa Rica have a recurrence interval of approximately 21 months (Jiang et al. 2012, Xie et al. 2020) with equivalent moment magnitudes up to 7.2. Also, SSE catalogues consist of relatively large SSEs (M_W ≥6.6) that occurred from 2002 (Xie et al. 2020). However, we still have limitations in the catalogue particularly from a chronological point of view,the first network of GPS stations has been installed in 2002, but there is only a sparse distribution before 2007; and from a geographical point of view, most of the GPS stations are installed in-land on the Nicoya Peninsula. Because there are no seafloor geodetic sites, we have difficulty to capture total geodetic information on the seafloor above the interplate boundary. But the GPS stations on the Nicoya Peninsula have a closer access to the beginning of the subduction zone and allow to obtain additional information, in particular on the shallow SSEs. The largest earthquakes recorded in the area are of Mw 7.6 which can be considered small compared to other subduction earthquakes like Chile (e.g. Mw 9.5 in May 1960), and Japan (e.g. Mw 9.1 in March 2011). These observations question the interaction between the slow slip event cycle and the earthquake cycle as well as how the stress can be transferred between the two types of events. In Costa Rica, the shallow and deep SSEs occur at the same along-strike areas, and occur updip and downdip of the seismogenic zone. These two kinds of events are not acting the same on the interseismic locking, with deep events releasing more locking downdip of the earthquake, then limiting the downdip rupture and by the same

Year	Magnitude	Depth	Region
1853	Ms > 7.5		Osa
1882	Ms > 7		Nicoya
1900	Ms 7.2		Nicoya
1916	Ms 7.4		Nicoya
1939	Ms 7.1		Nicoya
1941	Ms 7.5		Osa
1950	Ms 7.7		Nicoya
1978	Mw 7.0	36 km	Nicoya
1983	Mw 7.1	28 km	Osa
1990	Mw 7.3	18 km	Nicoya
1999	Mw 6.9	24 km	Central
2012	Mw 7.6	30 km	Nicoya

Date	Duration	Depth	Region
2003	30 days		Nicoya
2005			
2007	30 days	6 km and 30 km	Nicoya
2009	6 months		Nicoya
2011	20 days		Nicoya
2012	6 months		Nicoya
2014	1.5 months	45 km	Nicoya
2015	7 months	10 km and 45 km	Nicoya
2017			
2019			

Table 1.1: Left: Summary of the larger earthquakes that occurred in Costa Rica along 3 main regions: Nicoya Peninsula, central part and Osa Peninsula. (CMT catalogue and Protti et al. (1994)), right: Summary of the SSEs that were registered in Costa Rica (Voss et al. 2017, 2018, Jiang et al. 2012, Outerbridge et al. 2010, Xie et al. 2020)

occasion the earthquake magnitude (Dixon et al. 2014). The two type of events seem to be associated with dehydration mechanism, with the updip transition zone corresponding to change in mechanical properties along the plate interface, with an increase of pore-fluid pressure due to basalt dehydration reactions, and the downdip transition zone corresponding to the range where low-grade metamorphic reactions occur (i.e. antigorite, lawsonite, chlorite and glaucophane) (Schwartz & DeShon 2007, Yamashita & Schubnel 2016).

Costa Rica can be divided into three main regions: North corresponding to the Nicoya Peninsula, central part and South corresponding the Osa Peninsula. These regions are divided mainly by the bathymetry of the subducting plate. The main differences between the three regions are: the age of the subducted slab ranges from 15-16 Ma in southern portion to 22-24 Ma in northern portion (Barckhausen et al. 2001); the oceanic lithosphere is rather rough with the existence of the Cocos Ridge in the south while the bathymetry is relatively smooth in the northern part and the central part is rough with the presence of some asperities; the velocity and direction of the convergence is different between the north and south portions as well as the dip angle which is steeper in northern Costa Rica. Also, an active volcanic arc is present in the north but not in the south (Norabuena et al. 2004).

The seismogenic zone limits slightly vary from north to south. Norabuena et al. (2004) studied the locked patched for both Nicoya and Osa peninsulas. For the Nicoya Peninsula, the transition zone between stable and unstable slip are centered at 14 $\pm$ 2 km depths and at 39 $\pm$ 6 km depth, marking the updip and downdip of the seismogenic zone (DeShon et al. 2006). Following the thermal evolution of Harris et al. (2010), these limits corresponds to $\sim$120-150°C and $\sim$200-250°C, respectively. For the Osa Peninsula, the seismogenic zone is shallower ranging from $\sim$ 10 to $\sim$30-35 km depth, for temperature varying from $\sim$100-120°C to $\sim$180-230°C. Arroyo et al. (2014) studied the central part of the Costa Rica Pacific margin. They found that the updip limit of the seismogenic zone is at 15 km depth with a temperature ranging from 100 to 120°C and a downdip limit around 25-30 km depth with a temperature ranging from 150 to 200°C. If uncertainties due to frictional heating are considered it could increase the transition temperature limit a little (Arroyo et al. 2014).

The recurrence interval of earthquakes changes between these three areas. There is a lack of SSE data for these three areas, but it is likely that the recurrence interval of SSEs is also different because of the difference in temperatures and thus seismogenic zones. The Nicoya Peninsula have registered most of the events both seismic and aseismic (Table 1.1). It is explained partly because this is where most of the seismic and GPS stations have been installed, because the Peninsula is really close to the Middle America Trench. Very few events have been registered in the central part, possibly because the GPS and seismic station installed on-land are far from the Middle America Trench. Also, the rough relief of the seamount domain in the central part of Costa Rica can reduce the coupling to patches that break generating moderate earthquakes (Protti et al. 1994) (e.g. 2002 Mw 6.4, 2017 Mw 6.5). The megathrust could also be smoothed by the accumulating slip developping corrugations, inhibiting rupture propagation (Kirkpatrick et al. 2020).

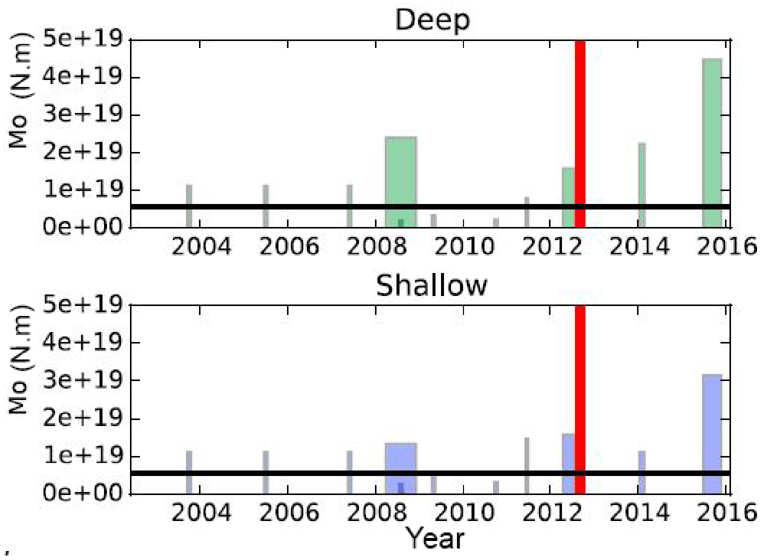

Figure 1.3: Shallow and deep SSEs in the Nicoya Peninsula, Costa Rica. Red rectangle represents the 2012 earthquake. Black horizontal line marks the assumed M6.5 detection treshold. From Voss et al. (2017)

From Figure 1.3, we can see that shallow and deep SSEs occur at the same time, with shallow SSEs having lower equivalent moment than the deep ones. A second study (Xie et al. 2020), also had the same observation, and added that deep SSEs last longer than the shallow ones. However, this study also highlights how challenging GPS study can be in Costa Rica because of uncertainties linked to variable atmospheric delay in tropical environment and to seasonal variations in surface deformation.

1.4 Numerical Models

Numerical modeling is not a tool for fitting models to nature but a research instrument to understand how nature works. With this in mind, numerical modeling have been used many times to study the evolution of the earthquake cycle in specific areas (Liu & Rice 2007, 2009, Lapusta et al. 2000, Li & Liu 2016, Yu H. 2018). They have presented some really interesting results using classic rate-and-state friction law created from laboratory experiments. It has shown real great capacity to model earthquake cycle from laboratory scales to real earthquake scales, both in 2D and 3D (Ampuero & Rubin 2008), and led to the current understanding of important processes leading to and resulting to an earthquake (Barbot et al. 2012).

One classical method to model earthquakes and SSEs is to use a predefined discrete fault embedded in a homogeneous elastic medium (Rice 1993, Lapusta et al. 2000, Liu & Rice 2007, Lapusta & Liu 2009, Li & Liu 2016, Yu H. 2018). It uses rate-dependant friction (Ampuero & Rubin 2008) implying that the internal friction coefficiant along a fault stongly depends on the fault slip rate and can either increase (velocity strengthening) or decrease (velocity weakening). It is typically assumed that slip along faults is governed by the rate-and-state dependent friction (Dieterich 1979, Ruina 1983). This friction simulation is based on the slide-hold-slide and velocity stepping rock lab-experiments (Dieterich 1979, Marone 1998). The used algorithm allows to treat accurately loading intervals of thousand of years and to calculate an entire seismic cycle with aseismic slip prior to dynamic rupture, the nucleation of an earthquake and the rupture propagation, the post seismic slip, for the earthquake and the SSEs. The methodology can be used to study a number of important question such as the fault behavior under low stress, the earthquake and SSE propagation, the interaction and evolution of SSEs during the seismic cycle.

In our case, we worked with a 1D fault embedded in a 2D model with depth-variable properties. Our choice to work with a 2D rather than a 3D model was based on several considerations: (1) the 3D modeling of the Costa Rica subduction zone was very computationally demanding (one simulation was taking weeks), (2) we would prefer to focus our study on the interactions between the seismogenic zone, and the transition zones where SSEs are formed. We would then be less interested in the impacts of the real 3D geometry of Costa Rica. Thus, in order to work with a good resolution of our model, compatible with a use of the characteristic slip distance L

rather low, working with a 1D fault integrated in a 2D model is a good compromise.

1.5 Thesis Outline

This thesis focuses on the relationship between slow earthquakes and megathrust ruptures, in the Costa Rica subduction zone where shallow and deep SSEs straddle the seismogenic zone. We also focus on the two distinct transition zones framing the seismogenic zone where respectively shallow and deep SSEs occur. Especially, we would like to adress the following questions:

- Can we find similar scale relationships between SSEs and earthquakes ?
- Could SSEs (shallow and/or deep) influence the nucleation of megathrust earthquakes in subduction zones and be used as a potential precursor ?
- How shallow and deep SSEs act in the seismic cycle ?

Chapter 2 focus on the scaling relationships of source parameters (stress drop, equivalent moment, magnitude, event duration) for SSEs from GPS inversion made in previous studies (LaBonte et al. 2009, Jiang et al. 2012, Dixon et al. 2014, Voss et al. 2017), and will apply to answer to the first question. This study shows the similarities and differencies in the empirical relationships between the SSEs source parameters of various subduction zones, and we add to it the study of Costa Rica that was not done before. We also study the differencies in the empirical relationships with earthquake ruptures. Our results showed that the stress drop in the Costa Rica subduction zone where following the same law as the stress drops of the previous studied area, with a stress drop of 2 order of magnitude lower than the earthquakes. Chapter 3 uses numerical modeling with the building of a 1D subduction earthquake cycle simulation code in the framework of rate- and state-dependant friction, and helps us answering the three other questions. SSEs have a periodic behavior that can be simulated with modeling of the earthquake cycle using a rate-and-state friction framework. We compiled the model results with various parameters to extract the recurrence interval, the average maximum slip velocity and the cumulative slip of SSEs and earthquakes, in function of these specific parameters. We then compare them to geophysical observations to be as close as possible to what is actually occurring in Costa Rica. Our study also highlights changes in the SSEs cycle before earthquake ruptures, which represents a major development in the modelling and the possible detection of earthquakes if these observation could be detected with GPS stations (Luo & Liu 2019). We also use the numerical model to study both the updip and the downdip transition zones where shallow and deep SSEs occur respectively to see if and how they interact with each other and with the nucleation of earthquakes. This is a quite innovative perspective in the modeling of SSEs since most of the SSEs that have been recorded before where mostly the deep ones, thus the models were mainly focusing on these ones.

2 Scaling Relationships of Source Parameters for SSEs in the Costa Rica Subduction Zone

2.1 Introduction

In seismology, it is of interest to know the properties (parameters) of an individual or a group of earthquakes. These source properties are: the difference in shear stress just before the rupture and/or fault slip and after the rupture and/or fault slip (static stress drop); the energy budget of the earthquake; the seismic moment; the rupture length; the rupture directivity; the rupture duration; the slip duration; discrimination of the fault plane from the auxiliary plane; and the corner frequency. These properties can be estimated by spectral analysis of P-waves and S-waves (Onwuemeka et al. 2018). A few studies have shown that these properties scale uniformly between earthquakes of different sizes in the same seismic volume, so we can use this scaling relationship (Allmann & Shearer 2009, Uchida et al. 2012). Especially, understanding any dependence of earthquake stress drop on tectonic setting is important for determining the factors controlling dynamic rupture, and for predicting future ground motion and seismic hazard (e.g. Field et al. (2015)).

In this chapter, we propose to follow the same kind of reasoning associated with SSEs rather than earthquakes and to compare our results with other studies.

The source parameters allow to have a better understanding of the factors controlling the rupture. Improving stress drop measurement and better quantifying the uncertainties involved are necessary steps to resolve the questions concerning the controls on earthquake stress release and rupture dynamics, and thus resulting seismic hazard. In this study, we want to compare the source parameters of earthquakes and slow slip events. This way, we will have a better understanding of the physical mechanisms of SSEs, and it will allow us to see if a correlation can be made between earthquakes and slow slip events. We focused our study in the compilation of the source parameters of the SSEs following equations and methods put in place in previous studies (Ide et al. 2007, Gao et al. 2012) and compare the results with source parameters of earthquakes and SSEs calculated in previous studies for different areas.

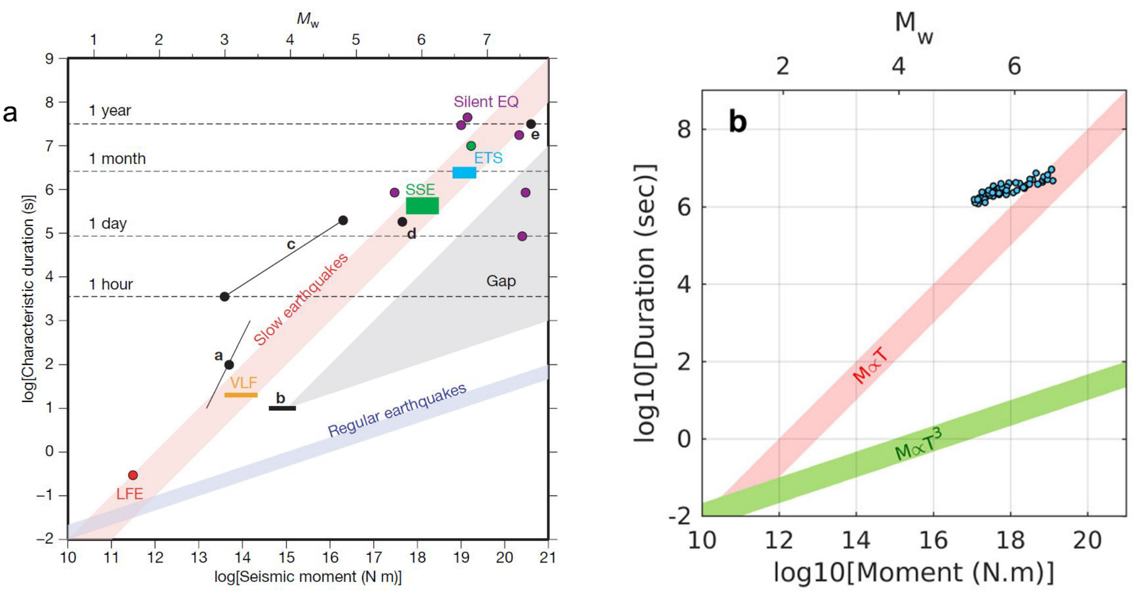

Figure 2.1: (a) Comparison between seismic moment and the characteristic duration of various slow earthquakes.The shaded red area represents the evolution of slow earthquakes, containing LFE (red), VLF (orange), SSE (green) and ETS (light blue) taken in the Nankai and Cascadia subduction zones.Purple plain circles are silent earthquakes, while black ones are slow events. The shaded blue area is the scaling relation for interplate earthquakes. From Ide et al. (2007) (b) Relationship between moment and duration for Cascadia SSEs, from Michel et al. (2019), red area is the linear scaling and green area is the cubic scaling.

Experiments made in laboratory have reported that rupture speed, on a continuum from SSE speeds to earthquake speeds, is controlled by shear stress drop (Leeman et al. 2016). The scaling relationship between duration and moment for SSEs is still unclear. Primary works based

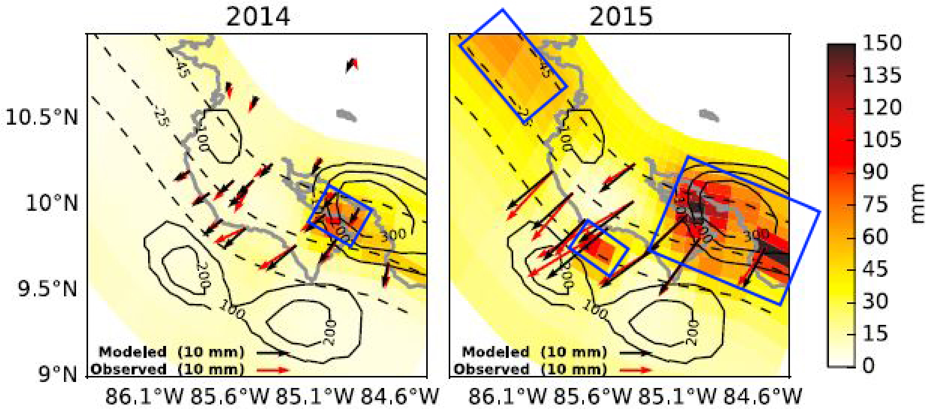

Figure 2.2: GPS inversions results of the 2014 and 2015 SSEs near Nicoya Peninsula from Voss et al. (2017) used to estimate fault dimension in this study. Colorbar is the slip magniude in mm. Dotted lines are the slab depths. Black contours represents the cumulative slip identified in previous SSE. Blue rectangles are drawn within which every GPS inversion grid has a total slip $\geq$ 5 cm, and define the respective SSE slip areas (length L and width W) in our compilation.

on observations compiled from various tectonic settings (Ide et al. 2007, Gao et al. 2012) have suggested that slow earthquakes follow specific scaling different from the earthquake scaling, even if their source is a shear slip for both of them, and proposed a general logarithmic scaling law of seismic moment M_0 and event duration T for SSEs, $M_0 \sim T$, different from the relationship observed for earthquake ruptures, $M_0 \sim T^3$ (Furumoto & Nakanishi 1983) (i.e Fig 2.1a)). This difference implies that to release a similar amount of energy, SSEs need a much longer rupture duration than earthquakes. Thus, the scaling and spectral behavior of slow earthquakes show that they can be thought as different modes of slip propagation.

However, a more recent study made in Cascadia (Michel et al. 2019), found that even for SSEs a cubic moment-duration scaling law is more likely, suggesting that the two kinds of events are governed by similar dynamic properties (i.e Fig 2.1b)). To do their study they used a recent catalog of surface deformation in Cascadia, and have deduced that the scale difference between SSEs and earthquake was probably due to catalogs dominated by unbounded ruptures whereas SSEs mostly represent bounded ruptures.

Previous studies did not look specifically at the Costa Rica subduction zone, but were rather focused on Cascadia and Nankai subduction zones. With this work, we complement this data gap by adding the Costa Rica subduction zone, and calculate how the source parameters in Costa Rica behave relative to other zones. Specifically, we used catalogs of source parameters data from previous studies for SSEs from 2000 to 2015 of M6.5+ in the Costa Rica area (LaBonte et al. 2009, Jiang et al. 2012, Dixon et al. 2014, Voss et al. 2017). From these catalogs, we extract the average slip area $\bar{D}$, the average rupture velocity V_r, the event duration T and the fault dimension, meaning the rupture area A to calculate the SSE equivalent moment M_0, the magnitude M_w and the static stress drop $\Delta\sigma$. Results are summarized in Table 2.1. We also want to have a better estimate of how the mechanisms of SSE and earthquakes might be related by examining the relationship between equivalent moment and slip area, the value of stress drop for SSE versus earthquakes, the evolution of equivalent moment with event duration for SSE versus earthquakes.

2.2 Source Scaling Relationships

We used empirical relationship between different source parameters. The empirical scaling relationships of earthquake source parameters provide important insights on constraints on the mechanics of earthquake rupture. We focus our study on two specific types of scaling : (1) equivalent moment vs total slip area, with the calculation of stress drops, and (2) equivalent moment vs event duration.

2.2.1 Equivalent Moment versus Slip Area

The relationship of seismic moment M_0 and fault area A has been explored previously for earthquakes (Kanamori & Anderson 1975):

$$\log M_0 = (3/2)\log A + \log \Delta\sigma + \log C \tag{2.1}$$

where C is a nondimensional factor for the fault shape, A is the fault area tha slip ($A = L \times W$), and $\Delta\sigma$ is the stress drop. This relationship assumes that the aspect ratio of a rupture patch is independent of magnitude, both for earthquakes and SSEs (Gao et al. 2012).
M_0 is defined as follow :

$$M_0 = \mu \bar{D} A \tag{2.2}$$

where μ is the shear modulus, $\bar{D}$ is the average displacement on the fault.

We used GPS inversion of 9 SSEs to calculate the source parameters and create a log-log relationship of the SSE equivalent moment and total slip area. Length and width of the slip area are compiled from the grids used in previous GPS inversions (Jiang et al. 2012, Dixon et al. 2014, Voss et al. 2017), as illustrated by the blue rectangles in Figure 2.2, for two examples in 2014 and 2015. Length is deduced from the along-strike dimension and the width is calculated from the depth of the event and the dip angle of the subducting fault. From these values, we made the assumption that the SSE slip area is rectangular, and we then obtain its size according to the equation $A = L \times W$. Specifically, we only took into account slip greater than 5 cm as it is considered to be the average resolution of inversion (Gao et al. 2012). Slab depth contours (dotted lines in Fig.2.2) gives us information about the depth at which SSEs are formed. Some cases studied had both shallow and deep SSEs, but most of them only had deep SSEs. We considered that the slip area, A, was the cumulative area of all fault patches that meet the criterion of slip greater than 5 cm. The average slip across area A is taken as the SSE slip, $\bar{D}$, in our source parameter scaling.

From the parameters extracted from the GPS inversion figures (i.e. $\bar{D}$ and A), we can calculate the equivalent moment (Eq. 2.2) from Aki (1966), using the characteristic dimension of the fault plane and the average slip amount. From the equivalent moment, we can calculate the moment magnitude (Eq.2.3) from Hanks & Kanamori (1979) as follow:

$$M_w = 2/3 \log(M_0) - 6.06 \tag{2.3}$$

where M_0 is in N-m. We can compare our results to the litterature, when possible, to verify if our extractions of $\bar{D}$ and A from the GPS inversions are correct.

In a second step, we calculate stress drops. to highlight differences or similarities between the stress drops of earthquakes and the stress drops of SSEs. In (Gao et al. 2012), we can see that the stress drops of slow slip events are of one to two orders of magnitude lower than for earthquakes (0.01 MPa to 0.1 MPa instead of 1 to 10 MPa for earthquakes). Adding Costa Rica to the study allows to see if this subduction zone follows the same scheme or acts differently.

For SSEs, we can estimate the stress drop using the equivalent moment M_0, the fault geometry, and the average slip area, following the equation of Kanamori & Anderson (1975) :

$$\Delta\sigma = \frac{C\mu\bar{D}}{L} \tag{2.4}$$

where C is a non dimension shape factor on the order of 1, μ is the shear modulus, $\bar{D}$ is the average fault slip and L the length of the fault, deduced from the GPS inversion grids. In our case, we assume μ to be equal to 40 GPa for all events. This value of shear modulus, chosen by Gao et al. (2012) for their calculation of source parameters, allows us to compare our results and add them to the scaling law graphs (Fig.2.3 and Fig.2.4). To calculate the stress drop scales represented by the slopes in Figure 2.3), we used the approximation of a rectangular fault with $L = 2W$. Previous studies (Kanamori & Anderson 1975, Geller 1976) have shown that the earthquake aspect ratio is found to be empirically constant, $L \sim 2W$, on average. Following the same idea, Gao et al. (2012), did the same work for various SSEs, and found that an aspect ratio of about 2 was best for describing the entire catalog of SSEs over a wide range of fault lengths.

Therefore, we used this scaling to derive the theoretical average stress drop calculation.

2.2.2 Equivalent Moment versus Event Duration

Ide et al. (2007) defined a linear scaling relationship between equivalent moment and event duration for SSEs, different that the cubic scaling relationship for earthquakes. A more recent study (Michel et al. 2019) defined the same relationship between equivalent moment and event duration for both earthquakes and SSEs : $M_0 \sim T^3$. We used previous studies to extract the duration of the SSEs. Duration varies from 25.5 days to 210 days (Table 2.1). We calculate the equivalent moment using Equation 2.2, and the GPS inversions defined previously. Then, we create a log-log relationship of equivalent moment to event duration, to explore the scaling of event duration and equivalent moment for SSEs.

2.3 Results

Results of our calculations of source parameters for 9 SSEs that occurred in Costa Rica between 2000 and 2015 are shown in Table 2.1. We have plotted the logarithmic relationship between equivalent moment and slip area from available data for SSEs in the Costa Rica subduction zone (Figure 2.3), and between event duration and equivalent moment (Figure 2.4), as this may help constrain the physical mechanism of SSEs. Our results are quite similar to studies on SSEs done for other subduction zones with low stress drops for SSEs in the 0.01 MPa to 0.1MPa range, close to the Cascadia and Japan SSEs, 1-2 orders of magnitude smaller than earthquakes. The duration-moment scale following the same linear trend that for the other SSE areas, and supporting the Ide et al. (2007) $\log M_0 \sim \log T$ trend, and most of our SSEs last between 1 month and 1 year for equivalent moments between 10^{19} N-m and 10^{20} N-m.

Reference	Date	M_w	M_0 (N-m)	$\Delta\sigma$ (MPa)	$\bar{D}$ (cm)	V_r (km/s)	A (km^2)	L (km)	W (km)	T (days)
LaBronte et al., 2009	2000	6.8			300	5.4e-06		12		25.5
Jiang et al., 2012	2003									30
	2005									30
Dixon et al., 2014	2007	7.0	4.6e19	0.03	12	5.8e-05	9600	150	64	30
	2009	7.3	1.2e20	0.016	13	2.1e-05	22720	320	71	180
	2011	6.9	3.1e19	0.011	7	1.8e-05	11262.5	265	42.5	170
	2012	7.2	8.2e19	0.012	9	1.9e-05	22720	300	71	180
Voss et al., 2017	2014	6.7	1.6e19	0.050	12	2.3e-05	3135	110	29	45
	2015	7.2	8.5e19	0.025	15	1.3e-05	14160	240	59	210

Table 2.1: Catalog of the source parameters used for the Costa Rica subduction zone.

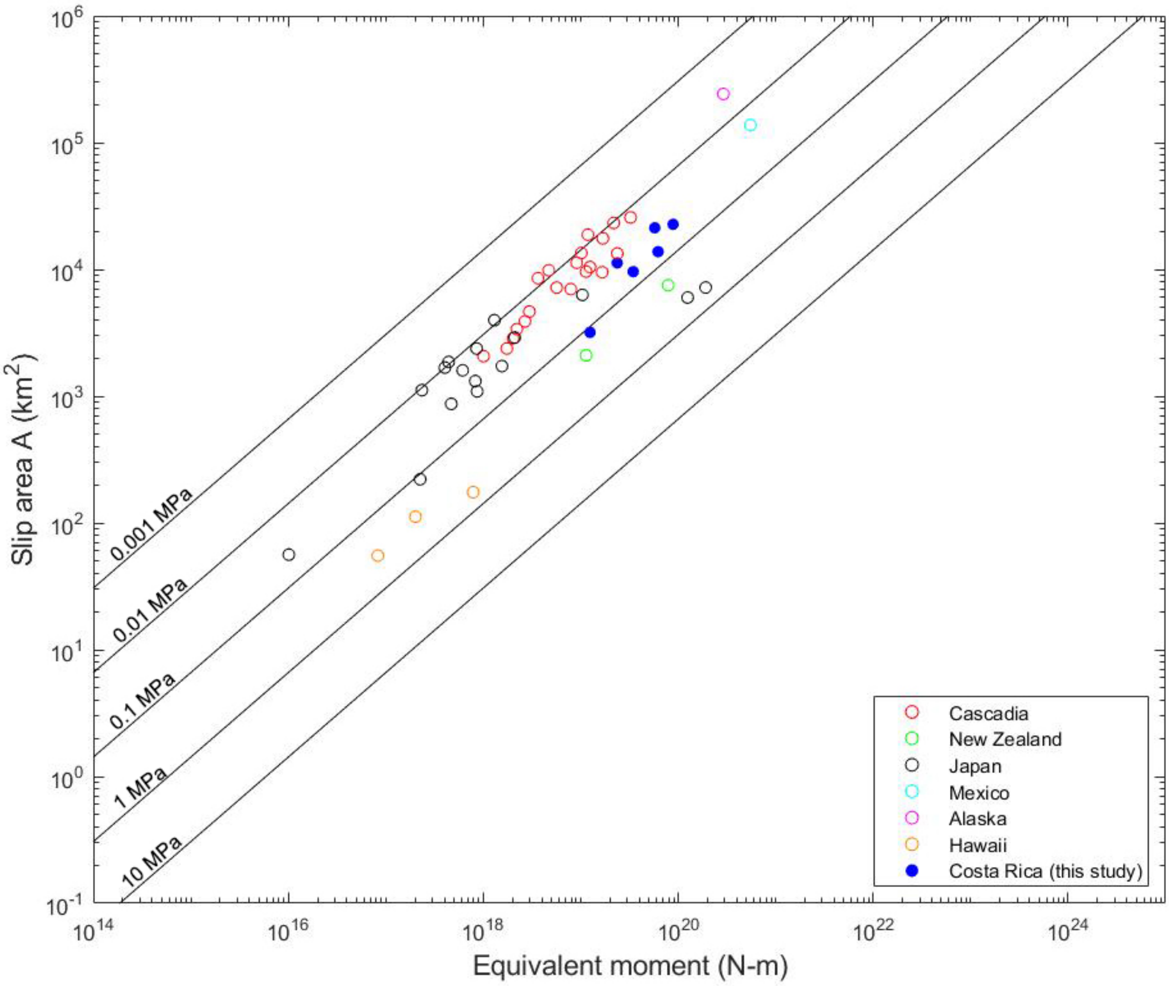

Figure 2.3: Results obtained from the calculation of the source parameters from GPS inversion (values shown in Table 2.1 for the Costa Rica and comparison with calculations of SSEs source parameters from other areas extract from supplementary table of Gao et al. (2012) and references therein. The slopes of average static stress drop are estimated by assuming $M_0 = \mu DA$, $\Delta\sigma = 16/(3\pi)\mu D/W$ and $L = 2W$. Straight lines represent the static stress drop $\Delta\sigma$ from 0.001 MPa (top line) to 10 MPa (bottom line).

2.4 Discussions and Conclusion

From Figure 2.3, comparing equivalent moment versus slip area, we observe that the Costa Rica subduction zone follows the same scale as SSEs taken in other regions, with a low stress drop between 0.01 and 0.1 MPa. And thus, parallels the log-log relationship of the earthquakes but

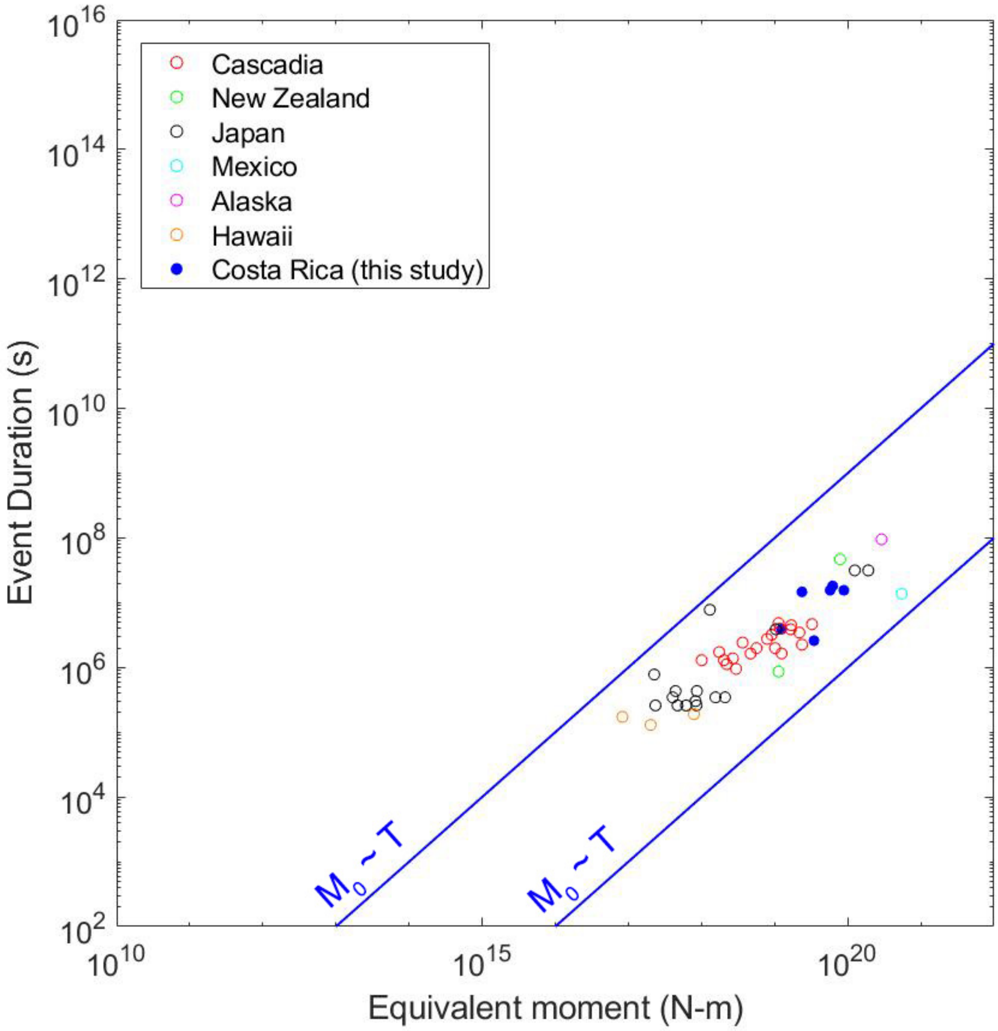

Figure 2.4: Results obtained from the calculation of the source parameters from GPS inversion (values shown in 2.1) for the Costa Rica and comparison with calculations of SSEs source parameters from other areas extract from supplementary table of Gao et al. (2012) and references therein. Logarithmic relationship between the duration of SSE and the equivalent moment. The strait lines indicate contours of constant event duration. SSEs event follow the $LogM_0 \sim LogT$ trend as shown by the blue lines.

1-2 orders of magnitude lower. Even though, as seen in Table 2.1, there are some variations in the rupture area and event size, however all SSEs are in the same range of 0.01 to 0.1 MPa, which leads to the idea that the stress drop for SSEs is independent of the rupture and event size.

From seismic observations, these low values of stress drops can be explained by the fact that SSEs occur in areas where pore fluid pressure is near-lithostatic due to metamorphic reactions (Audet et al. 2009), resulting in very low effective normal stress. The low estimate of effective normal stress limits the level of shear stress on the fault, and thus, might limit the stress drop.

For the scaling relationship between moment and duration, from our results on SSEs in Costa Rica, they appear to follow a linear scale between moment and duration, as proposed by Ide et al. (2007). However, we worked with very few events. More events might show a different pattern that might be more in line with the Michel et al. (2019) study and its cubic relationship similar to earthquakes. Part of the difference in the scaling law between earthquakes and SSEs can be explained by the aspect of the rupture where SSEs can be much more elongated than earthquakes (see Figure 1.2), and only partially slipping at one time compared to earthquake rupture. Also, Michel et al. (2019) worked on an updated catalogue of SSEs from Cascadia, that focuses on bounded ruptures. It is possible that the moment-duration relation shows variation among individual margins, corresponding to the scaling $M_0 \propto T^n$ with the scaling factor n varying between 1 and 3 (Ide et al. 2007, Gao et al. 2012, Liu 2014, Michel et al. 2019).

To go further, and as the study of SSEs in Costa Rica intensifies, we could add new GPS data where we can identify both shallow and deep SSEs. This would allow a true analysis of the source parameters of shallow versus deep SSEs.

3 Spatiotemporal evolution of shallow and deep SSEs in a Costa Rica planar fault model

3.1 Introduction

In this section, we investigate the physical mechanisms of shallow and deep SSEs and megathrust earhquakes and their possible relation by developping a 1D subduction fault model using the rate-and-sate friction law with friction parameters adapted for the Costa Rica subduction zone (Harris et al. 2010).

Numerical simulations in SSE source mechanism have shown that SSEs can be modeled as shear sliding on faults at depths of unstable to stable transitional behavior (Liu & Rice 2005, Rubin 2008) or a mixture of alternating stability properties (Skarbek et al. 2012), effective dilatancy strengthening under high pore pressure conditions (Liu & Rubin 2010), or through a combination of brittle and viscous material rheology (Reber et al. 2015). Most of the friction-based models involve near-lithostatic pore pressure condition at SSE source depths in order to modulate SSE durations and recurrence intervals.

SSEs can arise spontaneously in the rate-and-state friction model when we follow a condition of near-lithostatic pore pressure p, thus a very low value of effective normal stress ($\bar{\sigma} = \sigma - p$) in the transition zones, updip and downdip the seismogenic zone (Liu & Rice 2005). This low effective normal stress can also be explained physically, by the presence of high pore pressure due to fluids released from dehydration of sediments updip the seismogenic zone and metamorphic dehydration downdip the seismogenic zone (Schwartz & DeShon 2007). Previous studies using rate- and state- friction models have been applied to simulate the earthquake processes (Lapusta et al. 2000, Lapusta & Liu 2009), the spontaneous slow-slip processes (Li & Liu 2016, Liu & Rice 2007), and the triggering of SSEs by a previous earthquake (Wei et al. 2018).

To study the mechanisms and relationship between shallow SSEs, deep SSEs and earthquakes, we use a 1D subduction fault model, that allows high resolution and short computation time. This model allow to analyze the slow slip and earthquake processes, and to calculate their source parameters (i.e. recurrence interval, cumulative slip, duration, depth of nucleation). We focus both on shallow and deep SSEs, as well as the cycles of both SSEs and earthquakes and how all these events can be related.

3.2 Method

This section presents how the subduction fault was constructed and how the rate-and-state friction law and constitutive relations of the simulation were applied. The friction parameters, mesh generation, and model resolution to meet the requirements dictated by the constitutive equations and computational resources will also be detailed.

3.2.1 Governing Equations and Parameters

We assume the evolution of fault shear strength is governed by the laboratory-derived rate- and state-dependent friction law, which describe how friction coefficient evolve as a function of the fault slip rate V and the state of the frictional surface characterized by the asperity average contact time θ (Dieterich 1979, Ruina 1983).The rate-and-state dependent friction law has been widely applied to simulate seismic and aseismic slip in earthquake sequence models (Lapusta et al. 2000, Lapusta & Liu 2009, Li & Liu 2016, Wei et al. 2018, Yu H. 2018). Specifically, fault shear stress is the product between friction coefficient and effective normal stress $\bar{\sigma}$ ($\bar{\sigma} = \sigma - p$ denotes the difference between normal stress and pore pressure).

$$\tau = \bar{\sigma}[f_0 + a\ln(\frac{V}{V_0}) + b\ln(\frac{V_0\theta}{L})] \tag{3.1}$$

where a and b are the non dimensional stability parameters, L the characteristic slip distance over which the state variable θ evolves, and f_0 is the friction coefficient at a reference velocity V_0 for steady-state slip. The friction law can follow various state evolution laws that parameterize the change in θ as a function of time (Bhattacharya et al. 2015). The more common laws are the slip law (Ruina 1983) and the ageing law (Dieterich 1979). Here the state evolution variable is following the ageing law, stating that friction evolves with time on stationary asperity.

$$\frac{d\theta}{dt} = 1 - \frac{V\theta}{L} \tag{3.2}$$

Both laws can and have been used to model earthquake and SSEs. It is important to choose wisely the state evolution law we are using, since it will have a main impact on the model (Rice 1993, Perrin et al. 1995). The aging law states the idea that friction can get restrengthened during quasi-stationary contact, with a focus on time dependence. While the slip law requires that all changes in friction must involve slip, focusing on the slip dependence.

Experiments controlling the slip and time aspects during slide-hold-slide tests (Beeler et al. 1994), showed that static friction change increased with the holding time, and that the data fixed the aging law much better than the slip law. Also, it has been demonstrated that the slip law can fit the symmetric step changes at both increasing and decreasing slip rates but fails to reconcile the time-dependant increase of shear strength (Ampuero & Rubin 2008) Finally, the slip law has been proved not suitable to reproduce the various source parameters of SSEs that inferred from GPS observations (Rubin 2008). Therefore, earthquake and SSEs cycle simulations commonly apply the aging law (Lapusta et al. 2000, Liu & Rice 2007, Yu H. 2018), and we have also used it in this thesis.

When $\frac{d\theta}{dt}$ = 0, the system is at steady-state:

$$\tau_{SS}(V) = \bar{\sigma}[f_0 + (a-b)\ln(\frac{V}{V_0})] \tag{3.3}$$

The stability of a fault is defined by the non-dimensional friction stability parameter $a-b$. It depends on the temperature, the rock type and the normal stress in friction experiments (Blanpied et al. 1998). We distinguish two specific cases:

- The case of $a-b$ positive implies that the fault is in stable condition, it means that the steady-state friction coefficient τ_{SS} increases with slip rate and the fault strengthen. Thus, it means that no nucleation will be created in this area, but that it can host transient when perturbed. Thus, we call it the velocity strengthening (VS) region.

- The case of $a-b$ negative, implies that the fault is in conditionally unstable conditions. The steady-state friction coefficient μ_{SS} decreases as slip rate increases and the fault weakens. If the fault size exceeds a specific value of critical stiffness k_c, spontaneous slip transients occur. We call it the velocity weakening (VW) region.

The rate-and-state friction law incorporates the characteristic slip distance L, that represents the characteristic slip required for the evolution of the state variable θ. The characteristic slip distance L is defined from slip evolution on laboratory rock experiments, and is on the order of tens of microns (Blanpied et al. 1995). In our model, we will vary this parameter from a constant 20 mm along the fault to a few millimeters when inside the shallow and deep transition zones (TZ1 and TZ2). The length of L, in the order of the millimiter, is much larger than typical experimental values ($\sim$ 5 to 100 μm), is constrained by computational limitations.

The depth-dependent $a-b$ distribution (see Figure 3.4) is obtained by converting frictional parameters measured from laboratory experiments on wet granite Blanpied et al. (1995) (see

Figure 3.1) using a temperature profile of the Costa Rica subduction fault (Harris et al. 2010). Harris et al. (2010) uses heat flow results to constrain thermal models of the Costa Rica subduction zone. We also observed the frictional evolution of gabbro (He et al. 2007) and basalt (Zhang et al. 2017) with temperature. However, although granite is not a material found in subduction zones, the evolution of its friction stability parameter $a - b$ with temperature, and thus with depth, was more consistent with the thermal evolution of the Costa Rica subduction zone (Harris et al. 2010). From $a - b$ laboratory experiments for wet granite (Blanpied et al. 1995), we observe a transition zone from positive to negative $a - b$ at 70-100 °C and a transition zone from negative to positive $a - b$ at 250-320°C, which is relatively close to the values where SSEs have been recorded in Costa Rica (6-16 km depth, corresponding to 80-175°C and 30-46 km depth, corresponding to 255-370°C). The evolution of these temperature profiles with depth is shown in Figure 3.2. We used data from earthquake and SSE source parameter studies to determine the depth interval in which earthquakes, shallow SSE, and deep SSE were recorded in the Nicoya Peninsula area (grouped in Table 1.1). Then we used the temperature profile of Costa Rica to extract the corresponding temperatures.

Finally, we compared our graph of temperature evolution along depth with graphs showing friction evolution made for different rocks in laboratory (e.g. granite, gabbro), in order to extract the friction evolution closest to what has been observed in Costa Rica.

In our case, we took the value of wet granite as its temperature evolution with depth is similar to the one of the Costa Rica subduction fault (Fig 3.1). Then we varied these $a - b$ values to be more in accordance with the temperature-depth evolution along the Costa Rica slab, as studied by Harris et al. (2010). Thus, we created five pivot points at five specific depths to represent the temperature dependent friction stability parameter at $(z, a - b) = (0, 0.004)$, $(16, -0.004)$, $(36, -0.004)$, $(46, 0)$,$(60, 0.005)$, where z is vertical depth.

The effective normal stress $\bar{\sigma}$ drop considerably in the transition zones where pore pressure

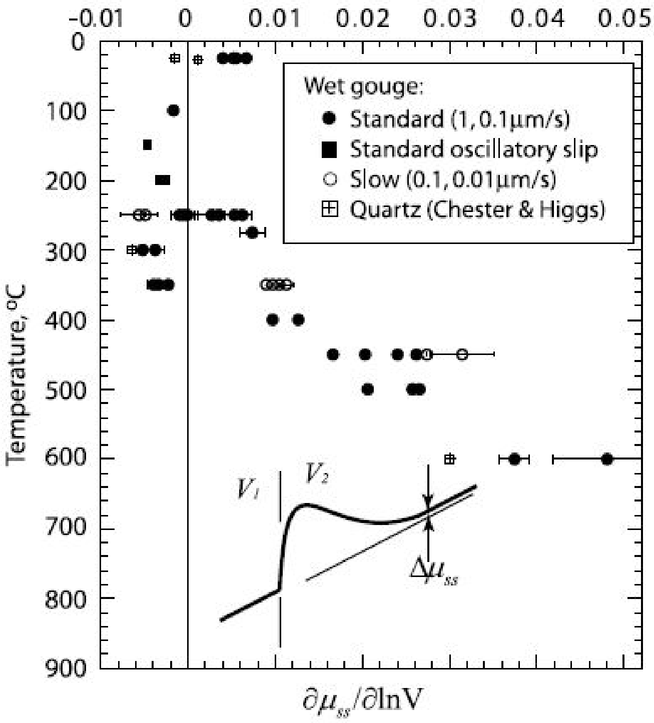

Figure 3.1: $a - b$ laboratory experiment for wet granite, from Blanpied et al. (1995). The solid vertical line marks the zero limit ($a - b$ = 0, neutral stability). Everything that is below zero ($a - b < 0$) will be velocity weakening, everything that is above zero ($a - b > 0$) will be velocity strengthening.

is assumed to be higher. In our model, we defined a constant $\bar{\sigma}$ of 35 MPa with a drop of value at the transition zones of a few MPa (0.7 to 3.5 MPa depending on tests).

We define 2 different thresholds for which we count the slip as spontaneous SSE. For the downdip SSEs, this occurence is defined when the maximum velocity exceeds $3V_{pl}$, where V_{pl} is the plate velocity. However, for the updip SSEs that have generally slower slip rates, we define this treshold at $1.5V_{pl}$. These thresholds allow us to ensure that we consider all SSEs for both shallow and deep. Using the same treshold value of $3V_{pl}$ would result in complete or partial loss of some slip stages in the updip transition zone SSEs in our numerical catalog. More details are shown when we discuss Figure 3.6.

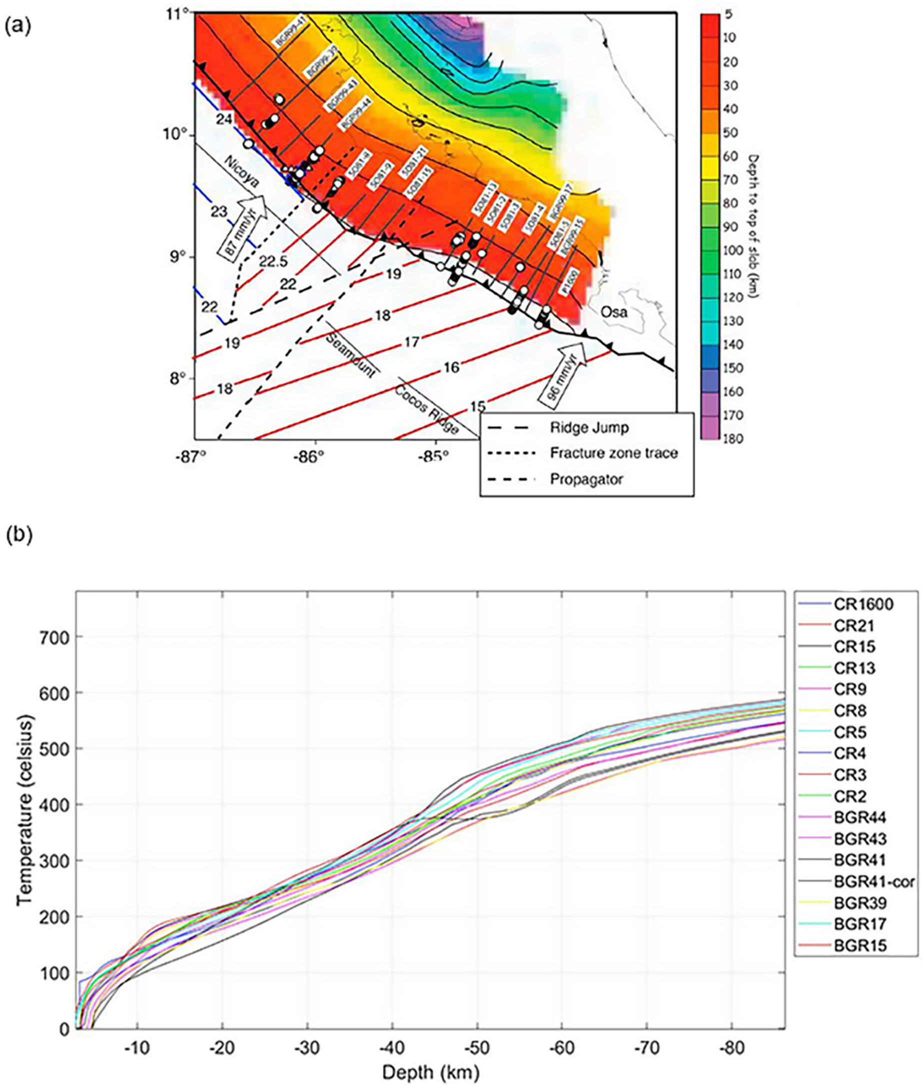

Figure 3.2: (a) Tectonic setting of the Costa Rica subduction zone. Color contours show the shape of the descending plate Ranero et al. (2005). The contour interval is 20 km. The positions of seismic reflection profiles are shown as solid lines, and heat flow profiles taken by Harris et al. (2010) are shown as white circles. (b) Relationship between temperature and depth from various profiles made by (Harris et al. 2010) along the Costa Rica subduction zone, shown in (a). X-axis is depth in km, Y-Axis is temperature in celsius.

We tested a few mesh sizes to observe the evolution of L, $a - b$ and $\bar{\sigma}$ and reproduce the average observations of recurrence interval, duration and maximum cumulative slip for earthquakes and SSEs. Taking into consideration both the numerical accuracy and the computation

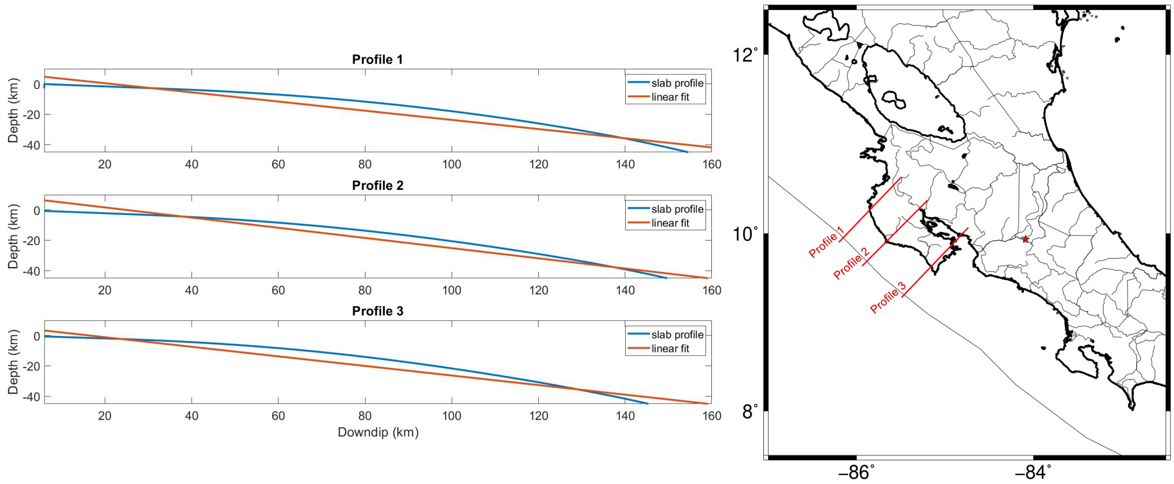

Figure 3.3: Three profiles taken along the Nicoya Peninsula part of the fault, from slab2 model (Hayes et al. 2018). The profiles along the Nicoya Peninsula are relatively similar with the dip angle ranging from 16° to 20°. Location of the profiles are shown on the map on the right. Red star represents the location of San Jose.

Steady state friction coefficient at V_0	f_0	0.6
Reference velocity	V_0	1 μm/s
Friction stability parameter	$a-b$	[-0.004,0.025]
Rate parameter	a	0.01
Characteristic slip distance inside TZ	L	0.2-1 mm
Effective normal stress inside TZ	$\bar{\sigma}$	0.4-3.5 MPa
Characteristic slip distance outside TZ	L	20 mm
Effective normal stress outside TZ	$\bar{\sigma}$	35 MPa
Shear modulus	μ	30 GPa
Poisson's ratio	ν	0.25
Characteristic nucleation size	h^*	8*h = 2 km
Grid size	h	0.25 km
Coseismic velocity threshold	V_{thres}	5 mm/s
Plate convergence rate	V_{pl}	84 mm/yr

Table 3.1: Summary of the parameters used in the 1D model of Costa Rica. TZ is the transition zone.

cost, we defined that a cell size of 0.25 km was a good choice for our simulation.

To realize the rate-and-state model of subduction zone fault with both megathrust earthquake and SSE regions, we used numerical evaluation of the rate-and-state equation with quasi-dynamic approximation, following the work of Rice (1993). This approximation results in slower rupture propagation, smaller slip rates and slip distance, while the rupture area and earthquake intervals are still comparable to those from fully dynamic simulations (Lapusta & Rice 2003).

$$\tau_i(t) = -\sum_{j=1}^{n} K_{ij}(\delta_j(t) - V_{pl}t) - \eta \frac{d\delta_i(t)}{dt} \tag{3.4}$$

where $\tau_i(t)$ and $\delta_i(t)$ are shear stress and slip on elements i, respectively. The Green's function K_{ij} is the stiffness matrix, which represents the shear stress change on element i due to a unit dislocation in the dip direction on element j. It is calculated in an elastic half-space medium (Okada 1992). The radiation damping factor $\eta = \mu/2c_s$, where μ is the shear modulus, and c_s is the shear wave velocity, is introduced to avoid unbounded slip rates during coseismic rupture (Rice 1993).

The above set of equations are capable of reproducing virtually the entire range of observed seismic and interseismic fault behaviors, from preseismic slip and earthquake nucleation to co-seismic rupture and earthquake afterslip (Marone 1998). In our case, we also have implemented spontaneous SSEs in the earthquake cycle. Laws include depth of seismic faulting, variations in the stability and seismic coupling at subduction zones and characteristic of aftershock rate decay.

We solved these equations by using a numerical code based on the Boundary Integral Method with adaptive time-stepping, developed by Lapusta et al. (2000) and Lapusta & Liu (2009). The Runge-Kutta method with adaptive step-size control is used to solve the couple ordinary differential equations (Stuart & Tullis 1995). Adaptive time stepping is crucial since it allows accurate resolution of both the nucleation and the developments of earthquakes.

Numerical Parameters

There are some numerical parameters that are essential to create ruptures in the simulation and that we will describe below.

The cohesive zone size Λ_0 gives the spatial length scale over which the shear stress drops from its peak to residual values at the propagating rupture front (Lapusta & Liu 2009). This length scale controls the numerical resolution during dynamic rupture. For the fault interface governed by linear slip-weakening law, Λ_0 can be expressed as (Palmer & Rice 1973)

$$\Lambda_0 = C_1(\frac{\mu^* L}{b\bar{\sigma}}) \tag{3.5}$$

where C_1 is a constant equal to $9\pi/32$ for linear shear stress drop (Palmer & Rice 1973, Lapusta & Liu 2009). For a 1D model, the ratio Λ_0/h can be quite large (between 5 to 10) to resolve dynamic rupture.

The nucleation size, h^*, is defined as the minimum dimension on the fault that would lead to a seismic rupture. It has been defined by Rice (1993), Lapusta et al. (2000) as

$$h^* = \frac{2\mu L}{\pi(1-\nu)(b-a)\bar{\sigma}} \tag{3.6}$$

where μ is the elastic shear modulus and ν is the Poisson ratio. In order to obtain convergent numerical results, this h^* is required to be much greater than the actual cell size $h = W_d/N$ (where N is the total number of cells along the fault, and W_d is the total downdip distance).In our case, we define $h^* = 8 * h$. Hence, the grid size h has to be small enough to resolve both Λ_0 and h^* and ensure continuum during dynamic rupture following this rule : $h^* > \Lambda_0 > h$ (Day et al. 2005, Lapusta & Liu 2009).

Finally, the length ratio W/h^* is a key parameter to determine the occurence of SSEs in subduction zones and to have qualitative response features of the model, as well as the behavior of the fault (Liu & Rice 2007). At least, four different regimes can be identify in function of the W/h^* ratio: (1) decaying oscillations toward stable sliding, (2) periodic aseismic slip transients, (3) periodic seismic slip and (4) aperiodic seismic slip affected by seismic waves reflected from model boundaries. In our model, we want to create both periodic aseismic slip (for SSEs) and periodic seismic slip (for earthquakes).

In order to find the optimal set of h^*, L and W that best reproduces the GPS observations, we explored the parameter space by independently varying the above three parameters to achieve a broad range of W/h^*, both for TZ1 (W_1/h^*) and for TZ2 (W_2/h^*) which strongly influences SSE source properties (Liu & Rice 2007, Rubin 2008, Liu & Rice 2009). A complete list of parameters and values used in the simulation is presented in Table 3.1. Wherever possible, values of parameters were chose to match values from appropriate laboratory experiments, or from observed geophysics studies.

3.2.2 Fault Slip Modeling in the Framework of Rate-and-state Friction

Based on the average properties of the region, we created a simplified subduction zone fault model that generates both megathrust ruptures and SSEs. The thrust fault between the subducting slab and the overlying continental plate can be simulated by a 1D planar frictional interface evolving only in the downdip direction in a 2D homogeneous elastic half-space.The parameters vary only in the downdip direction and with time. We created a mesh-grid in the downdip direction with cells of 0.25 km.

The 1D model we present here allows high numerical resolutions, allowing us to use relatively low characteristic slip distance values, closer to the ones calculated from laboratory, and relatively short computation time for the exploration of wide parameters range.

Because most of the SSEs were recorded beneath the Nicoya Peninsula, we investigate different profiles from Harris et al. (2010) along this area. From Figure 3.3, we can observe

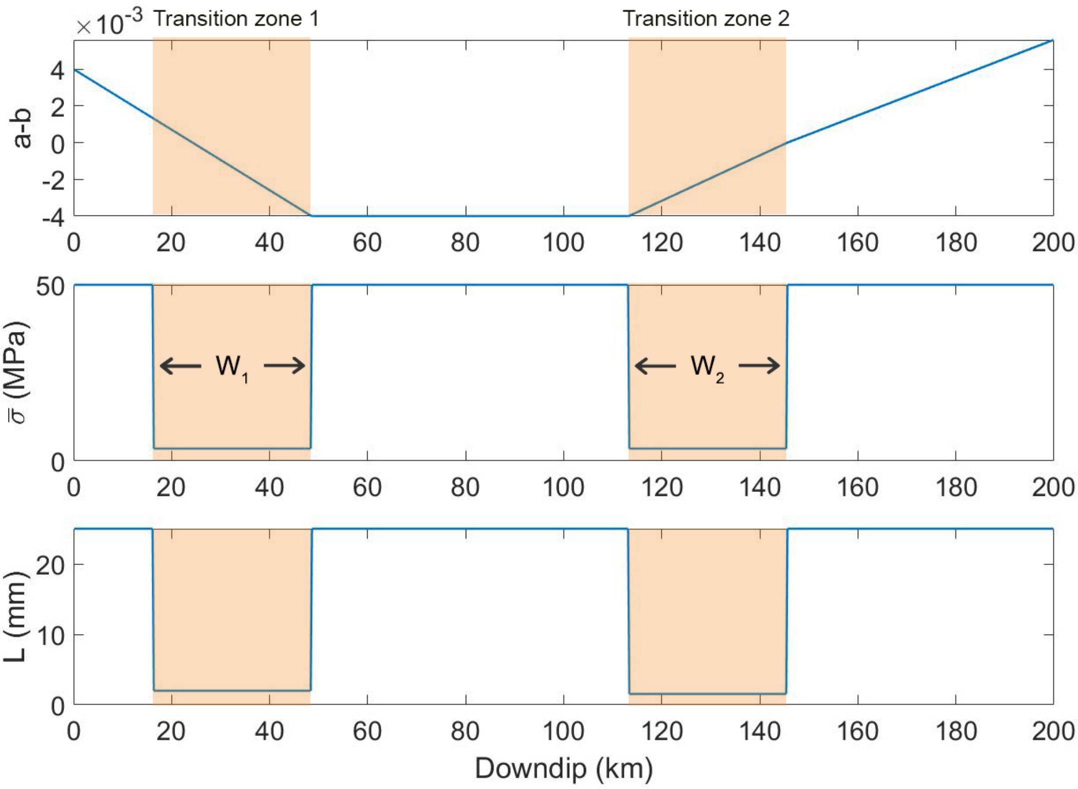

Figure 3.4: Downdip distribution of friction parameters $a - b$, effective normal stress $\bar{\sigma}$, and characteristic slip distance L. The low $\bar{\sigma}$ and L are combined with the transition from positive-negative $a - b$ and are where the SSE can arise spontaneously. Label W_1 and W_2 on the figure corresponds to the downdip distance of the Transition Zone 1 and to the downdip distance of the Transition Zone 2.

that the fault can be represented as linear with a dip angle between 16 and 20 degrees at the Nicoya Peninsula. We use the dip angle $\theta_d = 18°$, the plate velocity $V_{pl} = 84$ mm/yr, and a total depth of 60 km (or a downdip distance $W_d = 200$ km), to approximate those of the Costa Rica subduction zone. From Table 1.1, listing the source parameters of past earthquakes and SSEs, we observe the deeper SSEs occurred around 45 km depth, while megathrust ruptures occurred between 18 and 30 km depth. From these observations, we define a velocity weakening (VW) zone from 16 to 34 km depth where megathrust rupture can spontaneously occur, with one updip transition zone from 5 to 15 km depth, and one downdip transition zone from 35 to 45 km depth, where SSEs can spontaneously occur. Thus, we created two transition zones on the top and the bottom of the seismogenic zone (TZ1 and TZ2, Figure 3.4) where SSEs occur.

We change the values of the effective normal stress and the characteristic slip distance outside of the transition zones and inside the transition zones. Inside the transition zones, we fixed effective normal stress and characteristic slip distance as constants of very low values. Those are key parameters affecting the SSE recurrence intervals and slip rates (Liu & Rice 2007).

We did various tests to find the more accurate set of parameters, but as an example, Figure 3.4 show these variations, with the effective normal stress varying from 35 MPa to a few MPa, and characteristic slip distance varying from 20 millimiter to less than a millimeter inside the transition zones. We defined different values of effective normal stress and characteristic slip distance for TZ1 and TZ2 (Fig. 3.4), corresponding to the stability transition from positive to negative $a - b$ value updip and transition from negative to positive $a - b$ value downdip the seismogenic zone (i.e. W_1 and W_2) used to calculate the W/h^* parameter. In these transition zones, we create constant and low value of effective normal stress $\bar{\sigma}$ and characteristic slip distance L. The characteristic slip distance used for the megathrust rupture region ($L = 20$ mm) is still three order of magnitude larger than the laboratory suggested value. However, for the sake of computation efficiency, this kind of large L value is commonly used for generating megathrust earthquakes.To reduce the impact of the large value of L on the simulation, we also use large values of h^* in the range of a few kilometers, allowing velocity weakening regions to slip stably prior to earthquake nucleation (Liu & Rice 2005, 2007). We varied the parameters to find the most accurate configuration that was able to reproduce the recurrence interval cycle of 50 years for earthquakes and 22 months for SSEs (see Figure 3.9)

To model earthquake sequences, we used a quasi-dynamic approach and worked with variable time stepping. This allowed us to get through episodes of quasi-static deformation when the creeping is really slow, with large time steps, and also study the dynamic propagation with decreased time steps.

3.3 Results

3.3.1 Recurrence Interval and Maximum Slip Rate

We investigated the maximum slip rate and recurrence interval for both SSEs and megathrust earthquakes for different set of parameters. We modeled the fault slip and stress history for a period of 400 years, which is sufficiently long to represent fault evolution in the interseismic period and to include many SSEs and earthquakes.

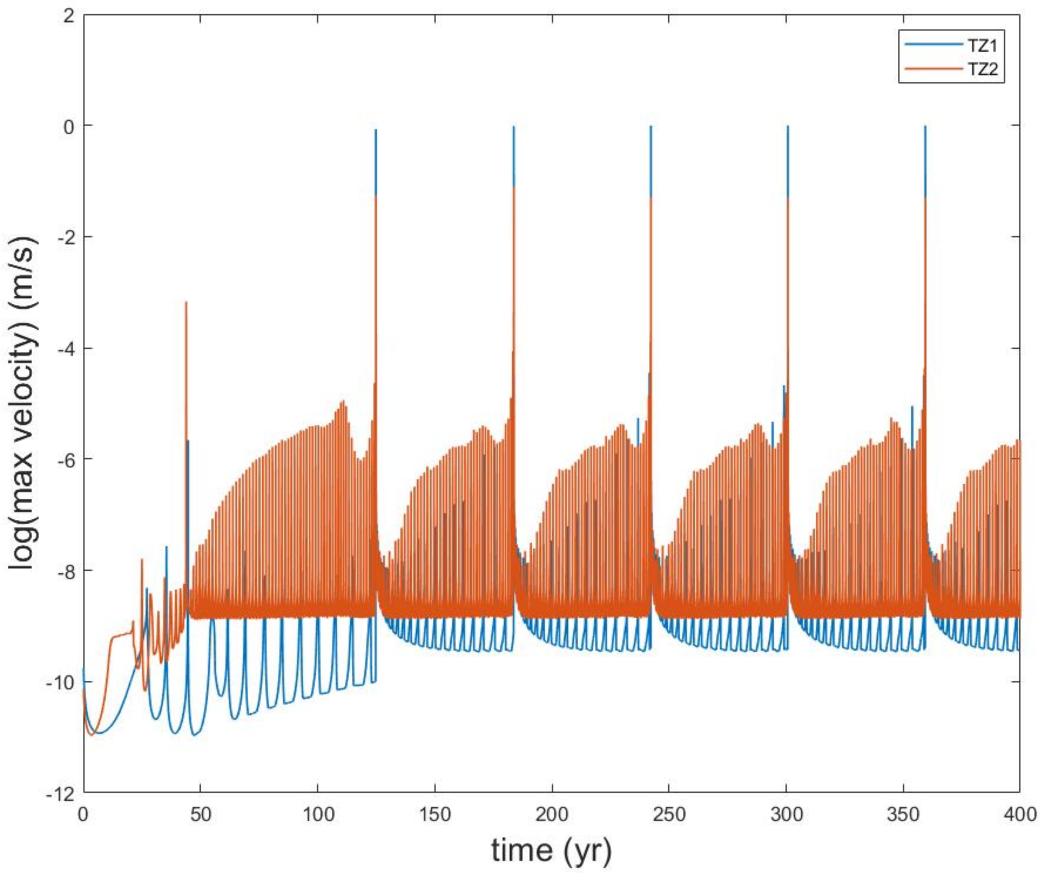

Figure 3.5: Fault slip rates during a 400 year simulation period for shallow (in blue) and deep (in orange) SSEs. Set of parameters for TZ1: L=0.5 mm, $\bar{\sigma}$=1 MPa. Set of parameters for TZ2: L=0.8 mm, $\bar{\sigma}$=2 MPa. Zoom in of TZ1 and TZ2 SSE slip rate histories are shown in Fig. 3.6.

Figure 3.5, represents the maximum velocity along the entire slab, for the full 400-year numerical simulation, of the shallow transition zone (in blue) and the deep transition zone (in orange). The high peaks with maximum velocity greater than 10^{-1} m/s represent earthquakes, while the lower peaks with maximum velocity less than 10^{-6} m/s represent SSEs. The plate velocity V_{pl} is equal to 84 mm/yr, or 2.6x10^{-9} m/s. The first cycle (the first 100 years) is not considered for the rest of the calculations because it seems to be the needed time for the model to stabilize. For the case shown in Figure 3.5, the effective normal stress varies from 35 MPa in the VS zone to 1 MPa in the VW zone for TZ1 and 2 MPa for TZ2, and the characteristic slip distance varies from 10 mm in the VS zone to 0.5 mm in the VW zone for TZ1 and 0.8 mm for TZ2. Here we observe 5 megathrust earthquakes in the total 400-year time range, with one earthquake about every 50 years and one SSE, in the downdip transition zone, every 20 months, which is close to actual observations of approximately 21 months (Jiang et al. 2012, Xie et al. 2020). The Figure 3.6 shows in detail a short period of time where several SSEs are recorded for TZ1 and TZ2, with the associated tresholds. For deep SSEs, slip is recorded as the cumulative slip on the fault when V_{max} exceeds $3V_{pl}$. For shallow SSEs, slip is recorded as the cumulative slip on the fault when V_{max} exceeds $1.5V_{pl}$. These thresholds allow the inclusion of the SSE nucleation phase as well as post-SSE relaxation. Because shallow SSEs have a lower maximum velocity, we set a lower threshold to be sure to detect all SSEs.

For the earthquake cycle, the values of effective normal stress and characteristic slip distance outside the transition zones have a huge impact on the recurrence intervals and the maximum slip rates, as can be shown in Figure 3.7. We observe that for higher values of effective normal stress $\bar{\sigma}$ and characteristic slip distance L the earthquake recurrence interval become larger, with one earthquake every 60 years in the configuration $\bar{\sigma}$ = 35 MPa and L = 10 mm, and one earthquake every 150 years in the configuration $\bar{\sigma}$ = 50 MPa and L = 25 mm. By varying a few times the parameters $\bar{\sigma}$, L and W/h^* (Figure 3.8) we were able to deduce that the optimal parameters

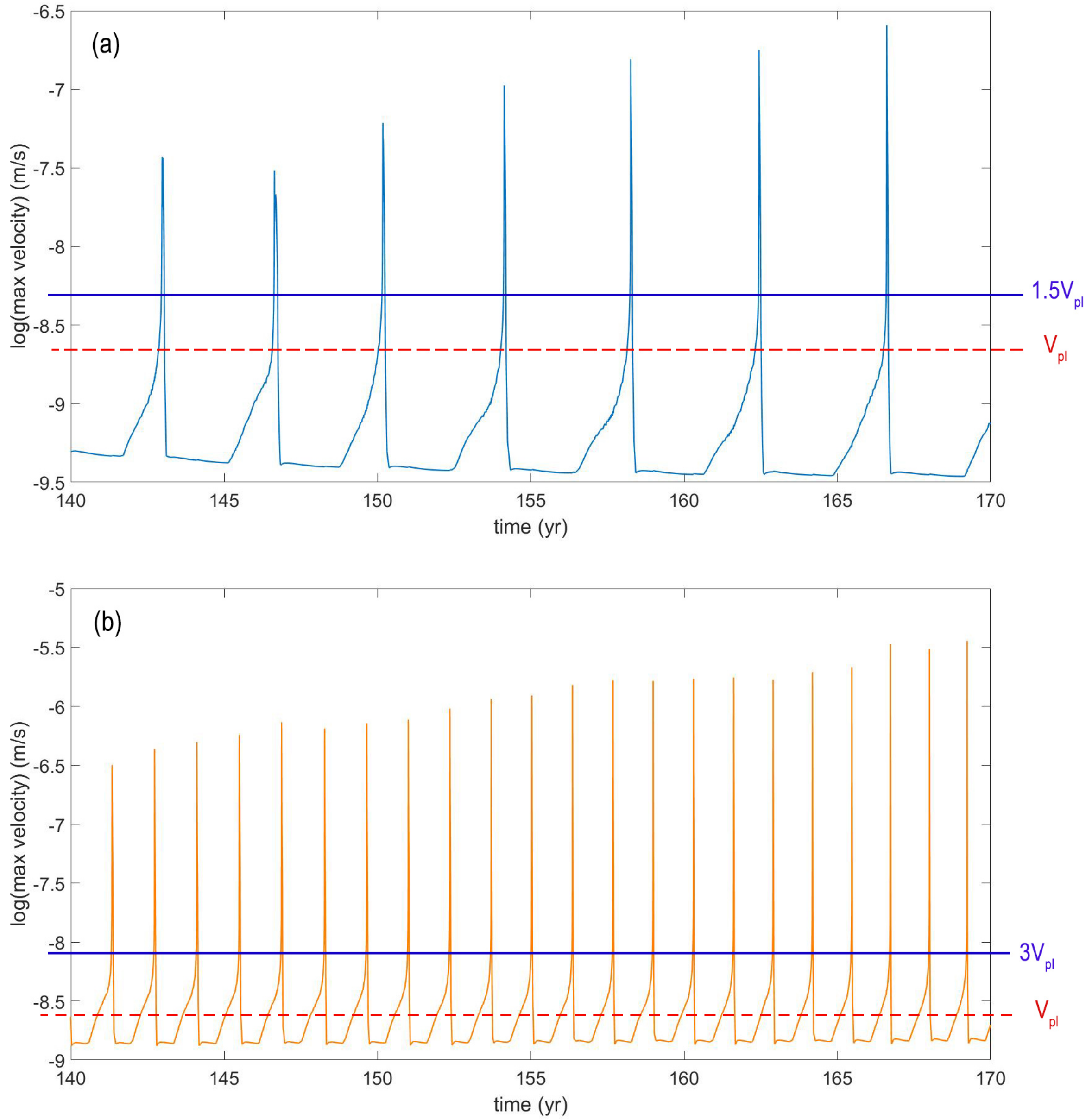

Figure 3.6: Zoom in of maximum velocity for a shorter period of time for SSEs. Red dashed line represents the plate velocity V_{pl} = 84 mm/yr. Blue line represents the treshold. (a) for transition zone 1, treshold is $1.5V_{pl}$, maximum velocity is from $10^{-9.5}$ to $10^{-6.5}$ (b) for transition zone 2, treshold is $3V_{pl}$, maximum velocity is from 10^{-9} to 10^{-3}.

to reproduce the recurrence interval cycle of megathrust earthquakes in the Nicoya Peninsula (one megathrust earthquake every 50-60 years) are $\bar{\sigma} = 35$ MPa, and $L = 10$ mm. Errorbar for

Figure 3.8 was obtained by computing the error bar from the complete 400-years seismic cycle, detecting all the earthquakes, and extracting the maximum interval and the minimum interval found between two earthquakes. This forms our error margin interval. We followed the same procedure for the maximum velocity error bars.

Unlike the Figure 3.7 which indicates that the lower the values of $\bar{\sigma}$ and L, the more earthquakes there will be in the same recurrence interval, we observe in Figure 3.5 and Figure 3.6, that more SSEs are recorded in TZ2, despite lower values of L and $\bar{\sigma}$ in TZ1. We can explain it because $a - b$ does not evolve in the same way in TZ1 and TZ2. The parameter h^* which is calculated as a function of a and b will therefore not have the same value in TZ1 and TZ2, and L scales with h^*. All this explains in part why for lower values of L and $\bar{\sigma}$ we can obtain larger recurrence intervals between two SSEs. But inside a same area (TZ1 or TZ2), the recurrence interval decrease with lower values of L and $\bar{\sigma}$.

From Figure 3.9, we were able to define the optimal set of parameters that could reproduce the actual recurrence interval in Costa Rica. Since our friction parameter $a - b$ evolves differently between TZ1 and TZ2 (c.f Figure 3.4), the optimal set of parameters are not the same updip and downdip the seismogenic zone. For all the cases shown in Figure 3.9 a)-e), it appears that to reproduce periodic SSEs of approximately 20 months, the W/h^* ratio must be between 0.8 and 1.2. If we look more closely, we can define with better accuracy the optimal L and $\bar{\sigma}$ parameters for TZ1 and TZ2, highlight in blue in Figure 3.9 c) and Figure 3.9 f). For transition zone 1, the optimal parameters are L ranging from 0.2 to 0.5 mm and $\bar{\sigma}$ ranging from 0.4 to 0.8 MPa. For transition 2, the optimal parameters are L ranging from 0.5 to 0.8 mm and $\bar{\sigma}$ ranging from 1.8 to 2.4 MPa. From Figure 3.10, we observe that cumulative slip is ranging between 2 to 5.5 cm. In Costa Rica, GPS observations have shown that cumulative slip for different SSEs varies between a few centimeters to tens of centimeters. If we follow the parameters that are optimal to reproduce the 20 months recurrence interval, we observe that this leads us to

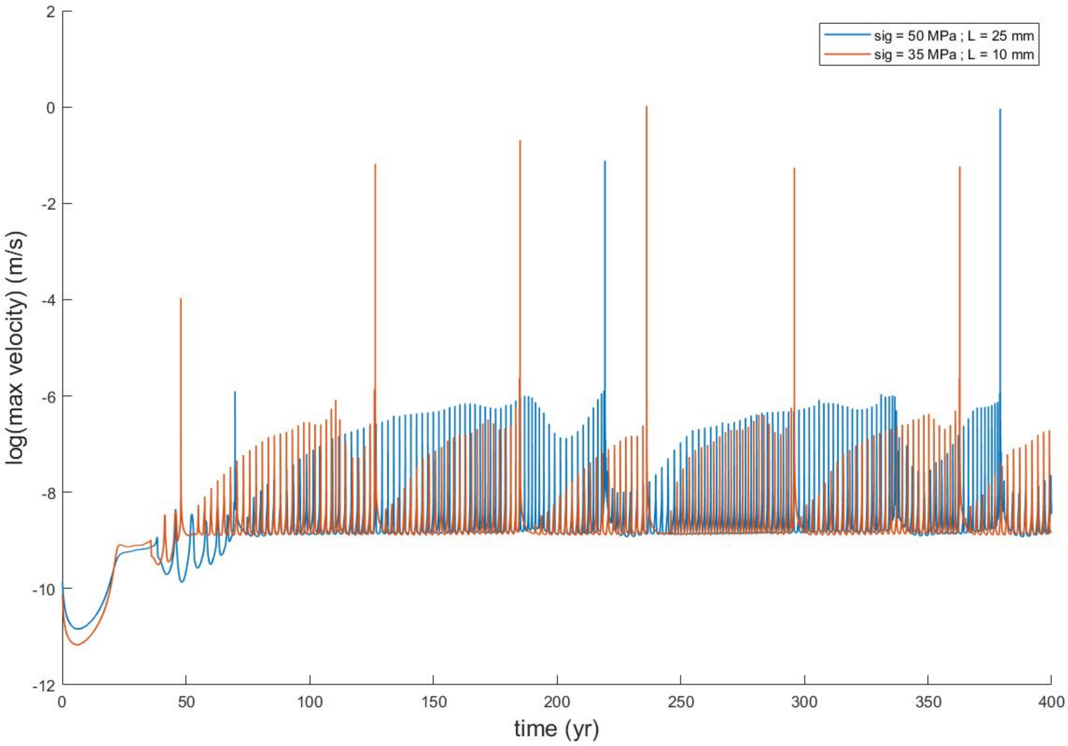

Figure 3.7: Maximum velocity versus time for two different set of effective normal stress and characteristic slip distance outside the transition zones. Blue line : $\bar{\sigma} = 50$ MPa , $L = 25$ mm. Red line : $\bar{\sigma} = 35$ MPa, $L = 10$ mm

small values of slip as shown by the blue oval areas shown in Figure 3.10, with cumulative slip ranging from 2 to 3.5 cm.

For a constant h^*, larger values of $\bar{\sigma}$ and L parameters lead to a larger recurrence interval between two SSEs and lower slip rates, as it was also observed in previous numerical studies (Liu & Rice 2007). An important part of the work was to find the best possible parameters to be accurate with geophysical observations.

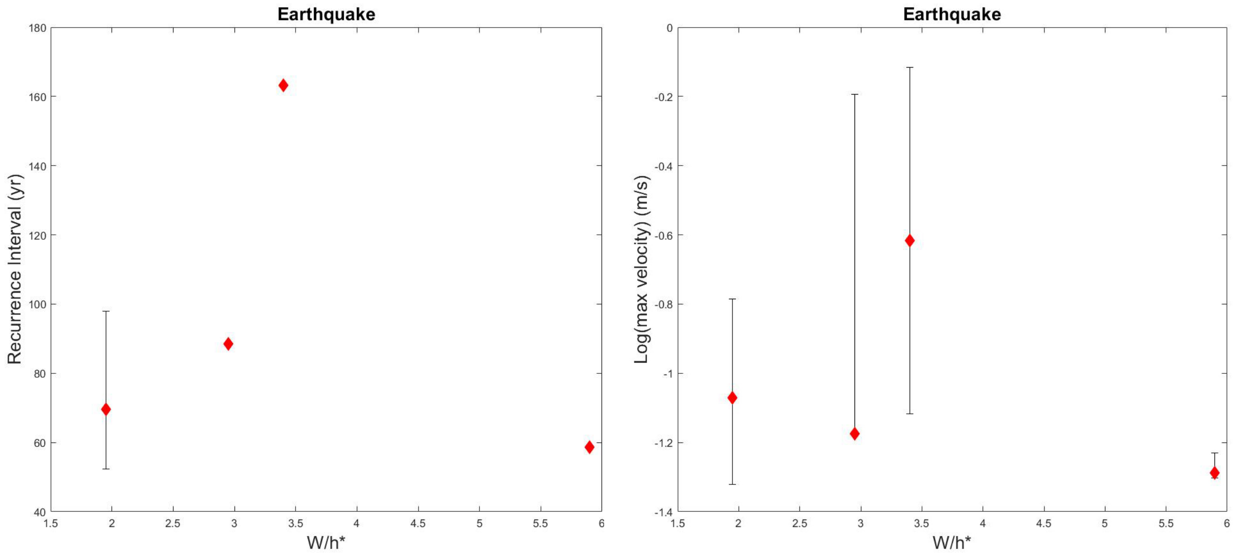

Figure 3.8: Modeled earthquake source properties of the seismic cycle for the entire 400 yr cycle (a) Recurrence interval (b) Maximum slip rate. For W/h^* = 1.95, $\bar{\sigma}$ = 50 MPa and L = 10 mm; W/h^* = 2.95, $\bar{\sigma}$ = 35 MPa and L = 20 mm; for W/h^* = 3.4, $\bar{\sigma}$ = 50 MPa and L = 25 mm; for W/h^* = 5.9, $\bar{\sigma}$ = 35 MPa and L = 10 mm.

3.3.2 Cumulative Slip

Figure 3.11 shows the cumulative slip along the fault for the simulated 400-year cycle of earthquakes and SSEs. The blue lines represent slip accumulation during interseismic periods plotted every 5 years, and the red lines show coseismic slip plotted every 1 second, when the slip rate exceeds 1 mm/s.

The entire velocity-weakening zone, from 45 to 90 km downdip, experiences significant and rapid coseismic slip, while very little slip occurs during the interseismic period. Above and below this zone is the velocity-strenghtening zone, which explains why no further earthquakes occur. The simulation produces a periodic sequence of five large events. From this figure, it is difficult to observe SSEs. For better observation, we present snapshots of SSE nucleation at specific times in the next section. We also represented the average slip rate on three different fault depth for the 400-year period, with five earthquakes and a zoom in of a period of 20 years

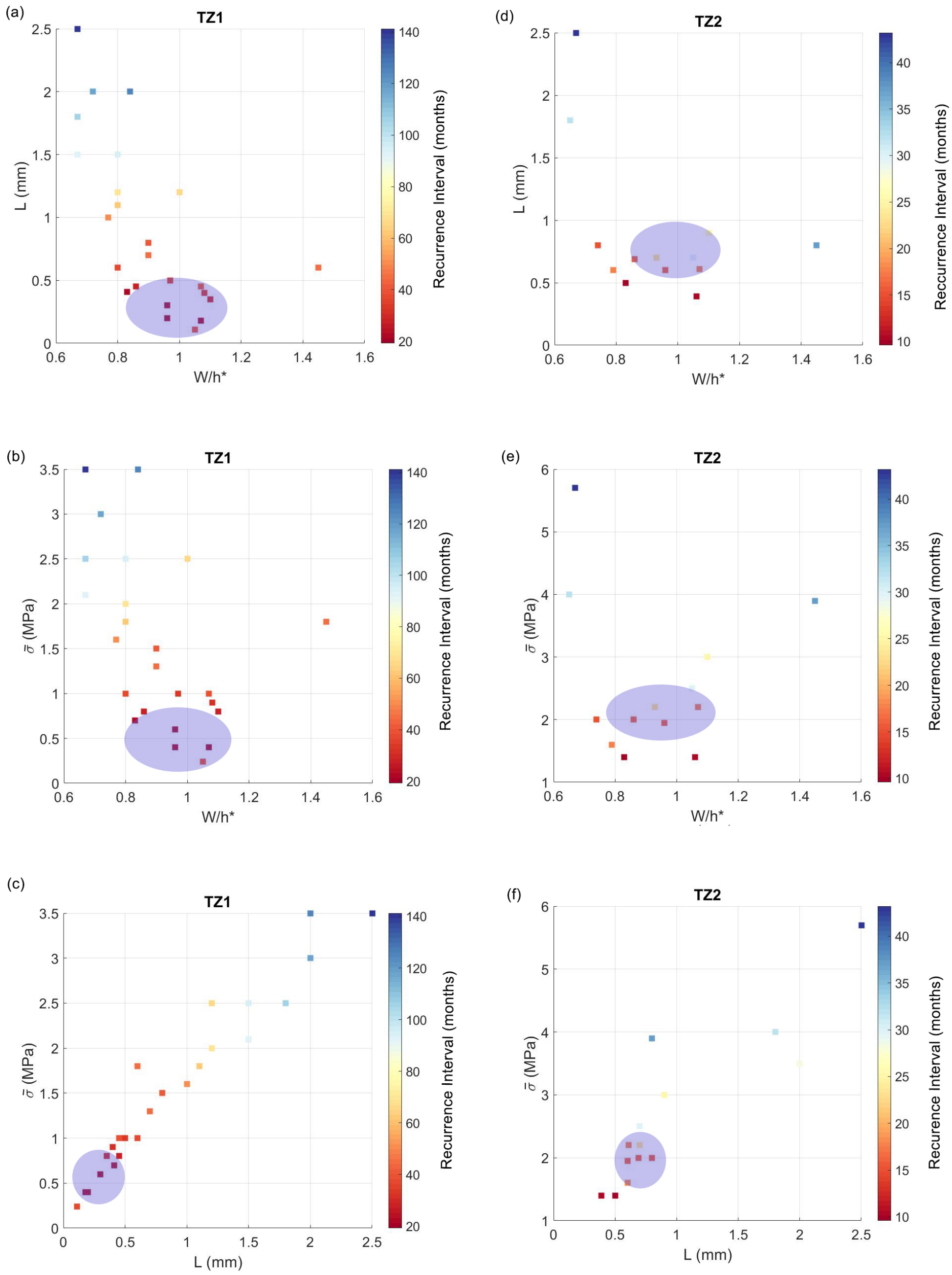

Figure 3.9: Phase diagrams of modeled SSE recurrence interval for TZ1 (left column) and TZ2 (right column). (a) and (d) L versus W/h^* ratio. (b) and (e) $\bar{\sigma}$ versus W/h^* ratio. (c) and (f) $\bar{\sigma}$ versus L. Colorbar is the recurrence interval in months. Blue oval areas highlight the optimal sets of parameters that are best reproduce SSE observations in Costa Rica.

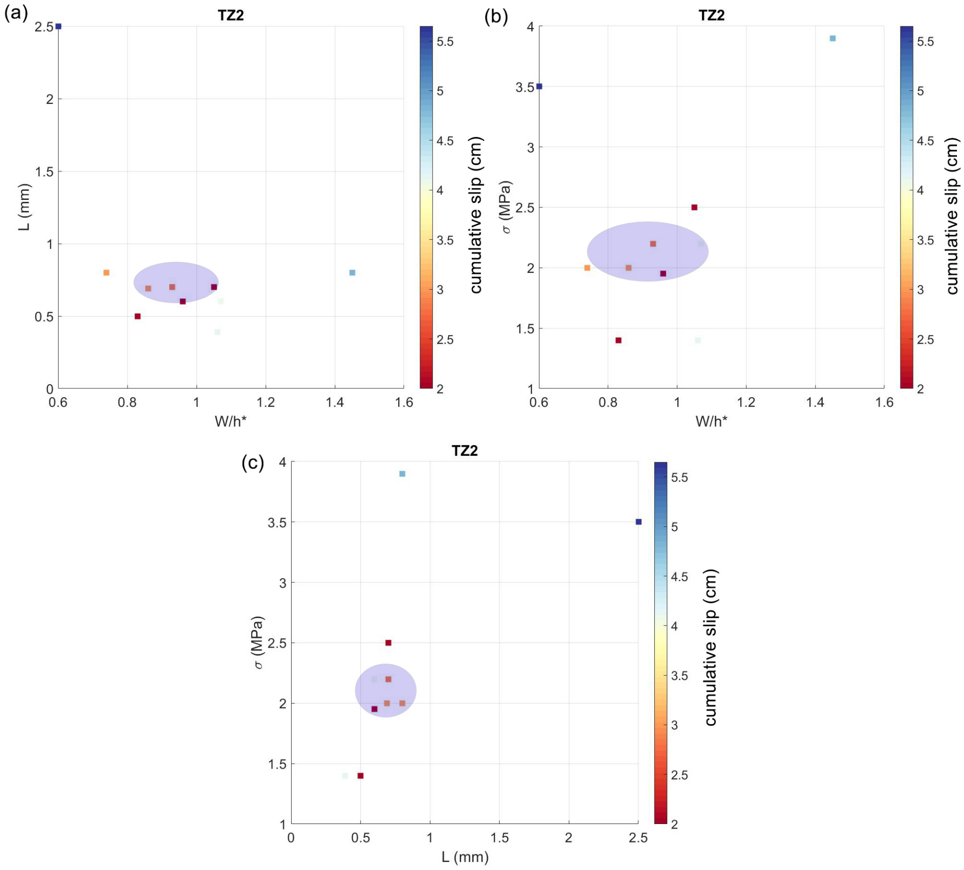

Figure 3.10: Phase diagram of modeled SSE cumulative slip for TZ2, the downdip transition zone. Colorbar is the cumulative slip in cm. (a) L versus W/h^* ratio, (b) $\bar{\sigma}$ versus W/h^*, (c) $\bar{\sigma}$ versus L. Blue oval areas highlight the optimal set of parameters that best reprouce SSE observations in Costa Rica, following Fig.3.9.

to observe the SSE slip (Figure 3.12). Average slip rate is appropriate to represent the energy release process (Liu 2014). We plotted the average slip for SSEs for z = 15 km (50 km downdip) corresponding to the TZ1, z = 25 km (83 km downdip) corresponding to the seismogenic zone and z = 40 km (133 km downdip) corresponding to the TZ2. The average slip is approximately 2 cm, which seems included in the GPS observations in the lowest bracket (e.g. 1.75 cm for the 2009 SSE, Jiang et al. (2012), 6 cm for the 2015 SSE, Voss et al. (2017), 11.8 cm for the 2007 SSE, Outerbridge et al. (2010)). A total of six SSE episodes occur during the 20-year time simulation, with regular recurrence interval of approximately 3 years and cumulative slip

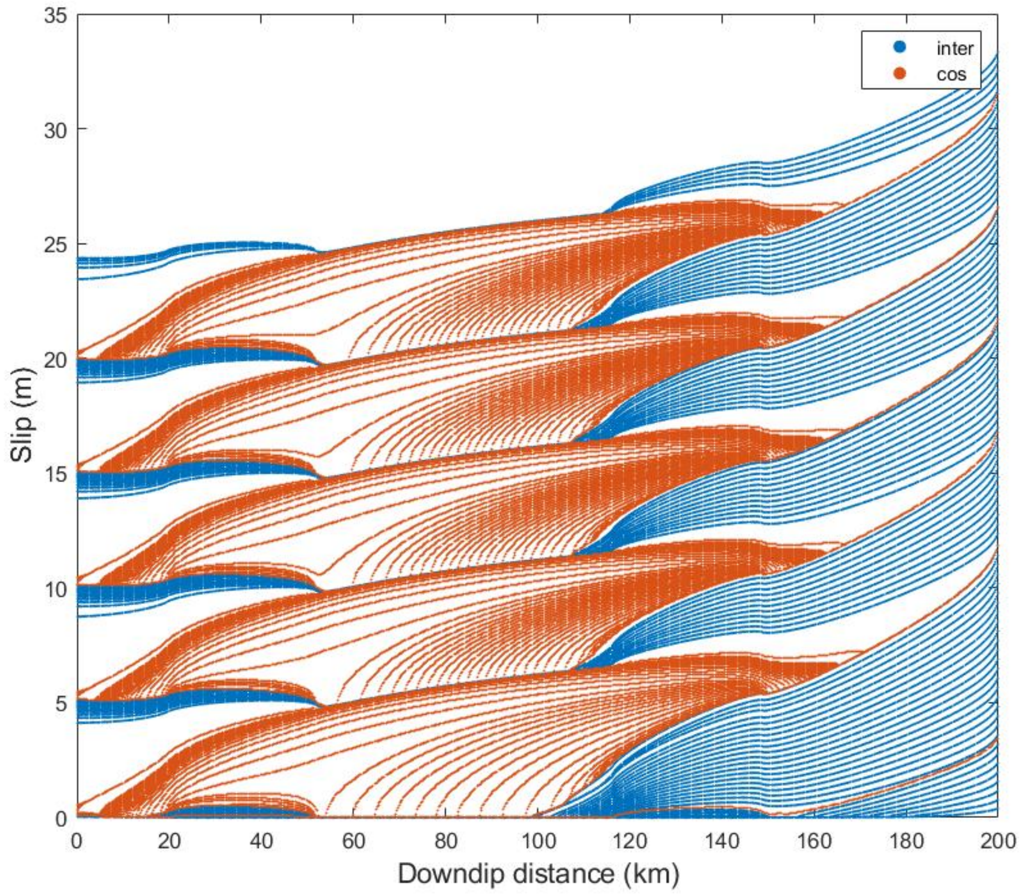

Figure 3.11: Cumulative slip along the Costa Rica subduction zone. The blue lines represent the slip accumulation during interseismic periods taken every 5 years and red lines represent the coseismic slip taken every 5 seconds, when the slip rate exceeds 1 mm/s

of approximately 2 cm.

3.3.3 Transient Slip Velocity Evolution

Figure 3.13 shows the slip velocity history of SSEs in a short period of time. It can be observed that shallow and deep SSEs do not have the same recurrence interval and do not act the same. For deep SSEs, there is a variation in velocity in the months preceding the earthquake and the propagation of the SSE occurs in both updip and downdip directions along the fault. Nucleation

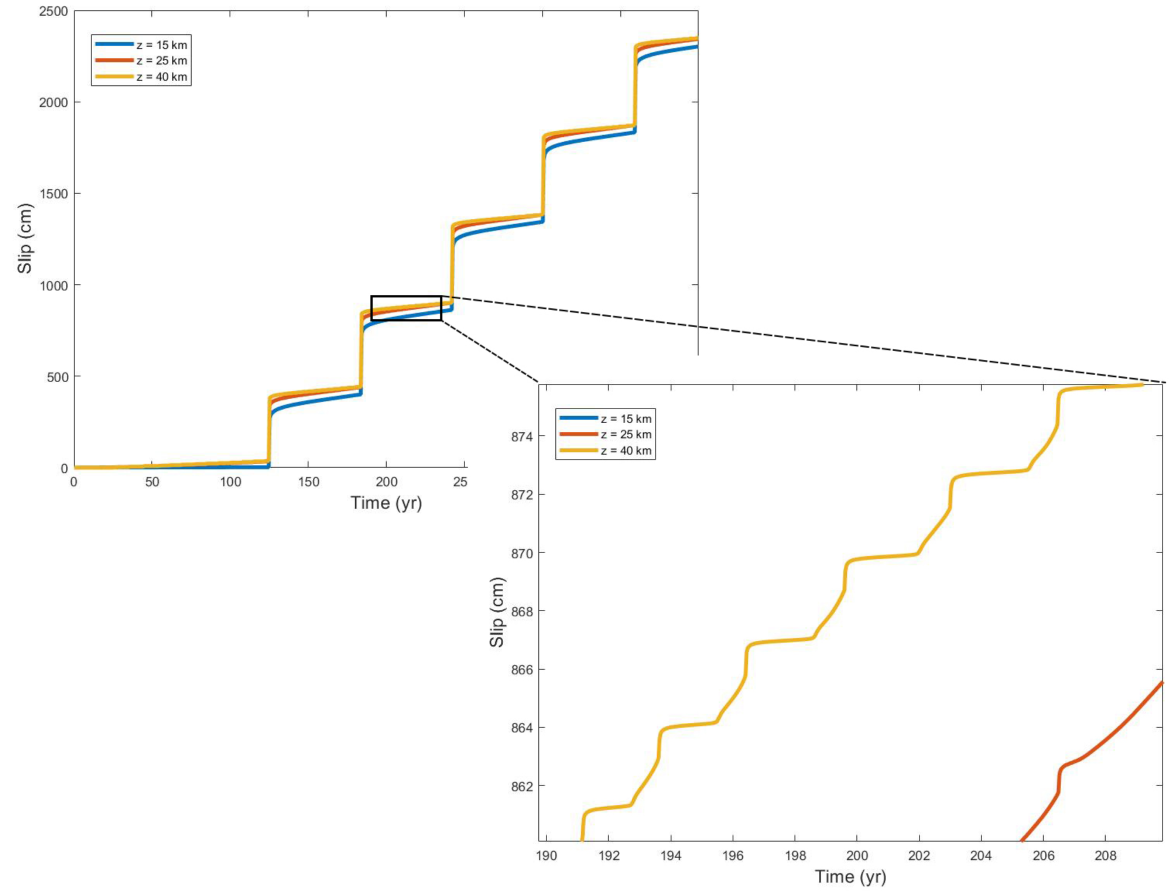

Figure 3.12: Slip at three distinct depths over the 400-year time periods with 5 earthquakes, and zoom in between t=190 yr and t=209 yr to observe SSE slips. The blue line is at z=15 km in the updip transition zone, the orange line is at z=25 km in the velocity-weakening region, z=40 km is in the downdip transition zone

propagates from about 115 to 150 km along dip and for about 0.11 years, or about 1.32 months. For the shallow event, we can see that the SSE extends over a larger time period and occurs less often. These kind of plots gives us information about the size of propagation, and the duration of the events. The duration of a SSE can vary inside the Nicoya Peninsula area, but from the litterature review of Costa Rica, summarize in Table 1.1, SSEs varies from 20 days to 7 months, with at least two deep SSEs lasting for at least 1 month (30 days in 2007, 1.5 months in 2014).

Thus, our snapshots seem to fit with GPS observations.

3.3.4 Variation between Updip and Downdip Transition Zones

As we saw previously, shallow and deep SSEs do not act the same.

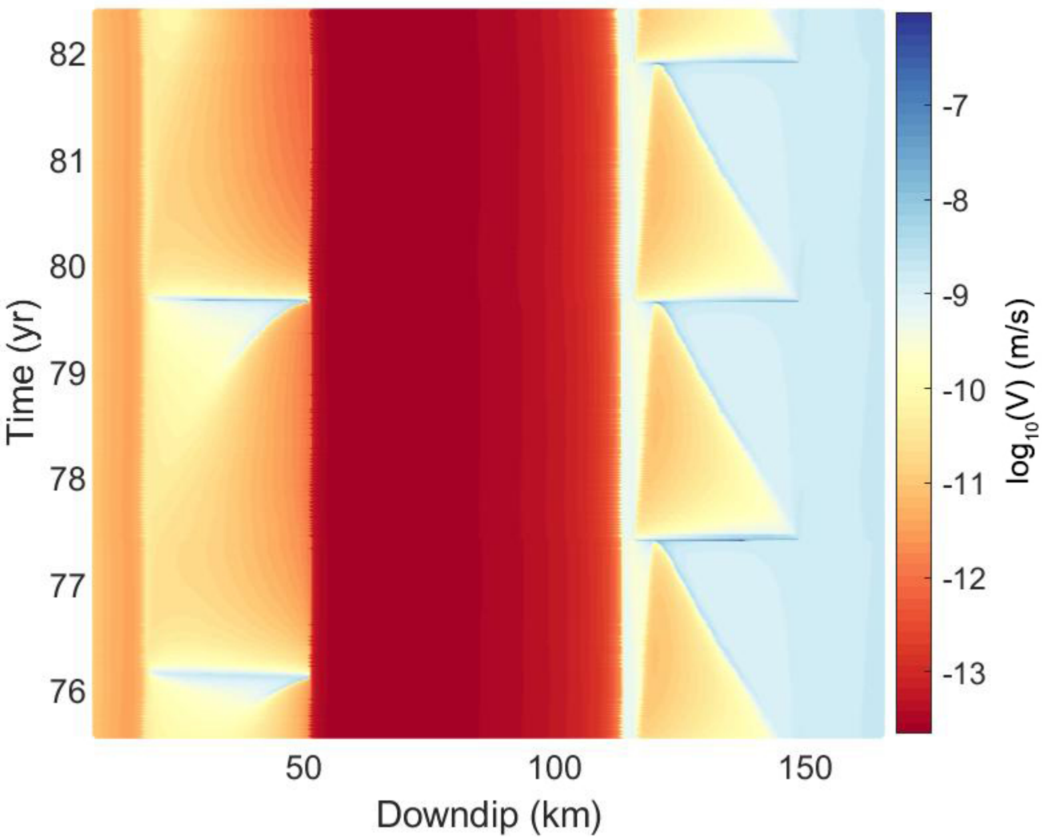

Figure 3.13: Slip velocity history during a specific time range where we can see one updip SSE and 5 downdip SSEs, with parameters h = 0.25 km, h^* = 8×h = 2 km. The term $log_{10}(V)$ in m/s is contoured along-dip.

Figure 3.13, representing a specific case, shows that for one shallow SSE, five deep SSEs are recorded. This value will depend a lot on the parameters chosen for the shallow transition zone, but in general, we record more SSEs downdip of the seismogenic zone than updip. We can also notice that both shallow and deep SSEs do not propagate in the seismogenic zone, so they do not influence each other.

We can relate some of our results to what is found in the GPS observations, in particular that there are more SSEs recorded downdip of the seismogenic zones than updip, for all subduction zones. We thought that this was mainly due to the lack of GPS near the subduction trench leading to a lack of data representing shallow SSEs. It appears, in our simulation, that this could also be related to the fact that there are indeed fewer spontaneous SSEs updip of seismogenic zones, that these events are longer but also slower than downdip SSEs, which makes them more difficult to observe with GPS stations. However, Voss et al. (2017) observed that shallow and deep SSEs occurred simultaneously in the few years prior to the 2012 earthquakes, but with lower slip velocity values. One explanation could be that some of the SSEs actually propagates through the seismogenic zone, which we did not model in our simulation.

3.3.5 Frequency Variation of SSEs as it Approaches the Next Megathrust

The behavior of the fault is strongly dependant on the characteristic slip distance, the effective normal stress and the ratio between the length of the rate-weakening section of the fault W and the nucleation length h^*.

We focused on a small range of time ($\sim$ 10 years) prior to the earthquake rupture, corresponding to a few SSE cycles before the earthquake, to see if there is a loading phase prior to the earthquake where the slip velocity and recurrence interval change. Figure 3.14, shows the zoomed in period of a few years before the earthquake. To the naked eye, we can see changes in the maximum velocity, with the maximum velocity for TZ2 decreasing slightly in the few SSE cycles prior to the earthquake. However, it is more difficult to see changes in the recurrence interval (the last SSE just before the earthquake does not count in the SSE cycle). We have therefore performed an analysis of SSEs simulated on several seismic cycles, which we have grouped in Figure 3.15. From this figure, we observe that there is a clear increase in the

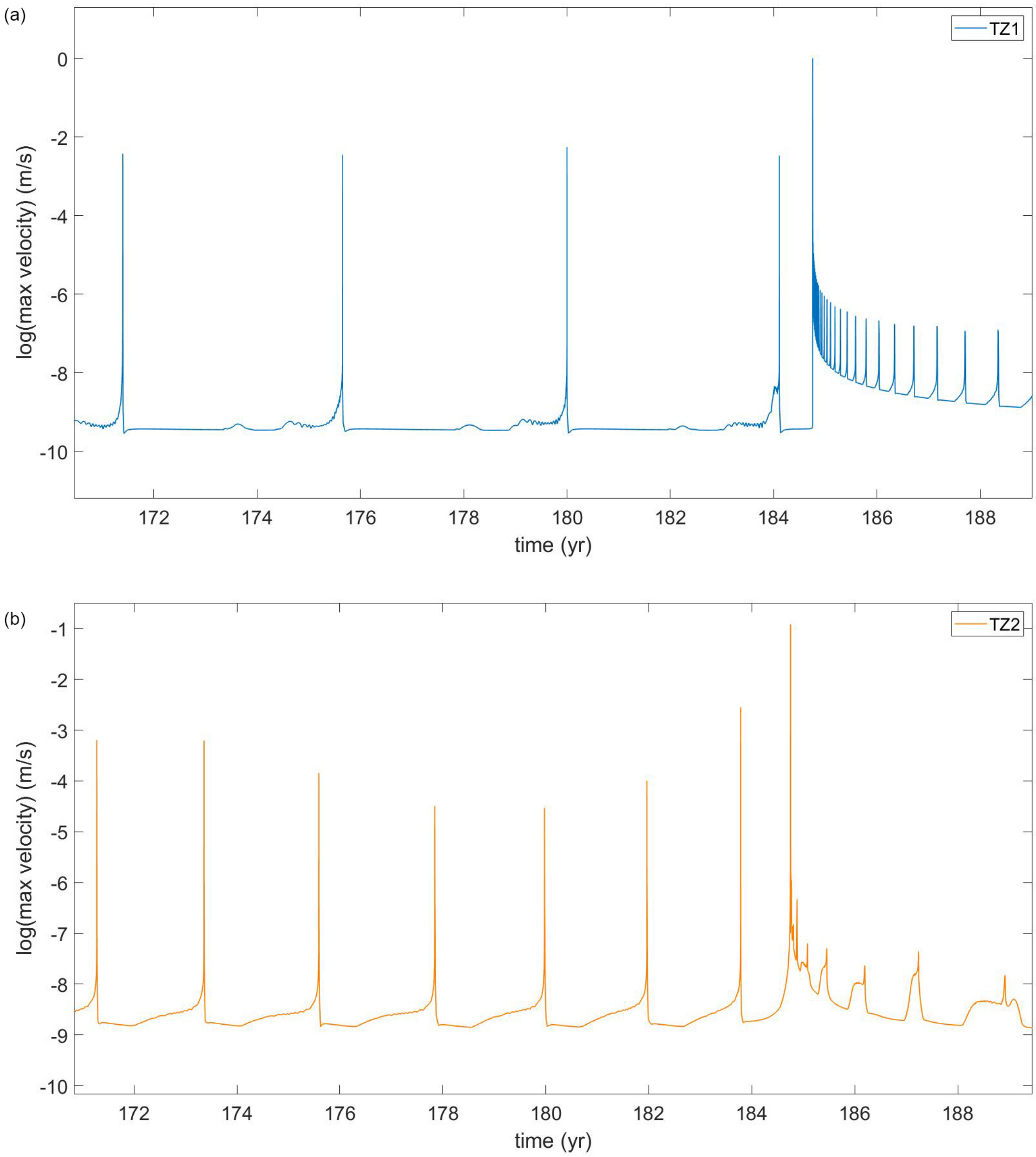

Figure 3.14: Zoom in of the maximum slip velocity of the 12 years before the megathrust rupture, for transition zone 1 (a) and transition zone 2 (b), with W/h^{*} = 1.

maximum velocity in the years preceding the earthquake, for both TZ1 and TZ2. However, for TZ2, in all the cases studied, we observed that the maximum slip velocity is very low after an earthquake and gradually increases, but in the pre-earthquake SSE cycles, this maximum slip velocity slightly decreases (as shown by the circled parts in Fig.3.16). This decrease in

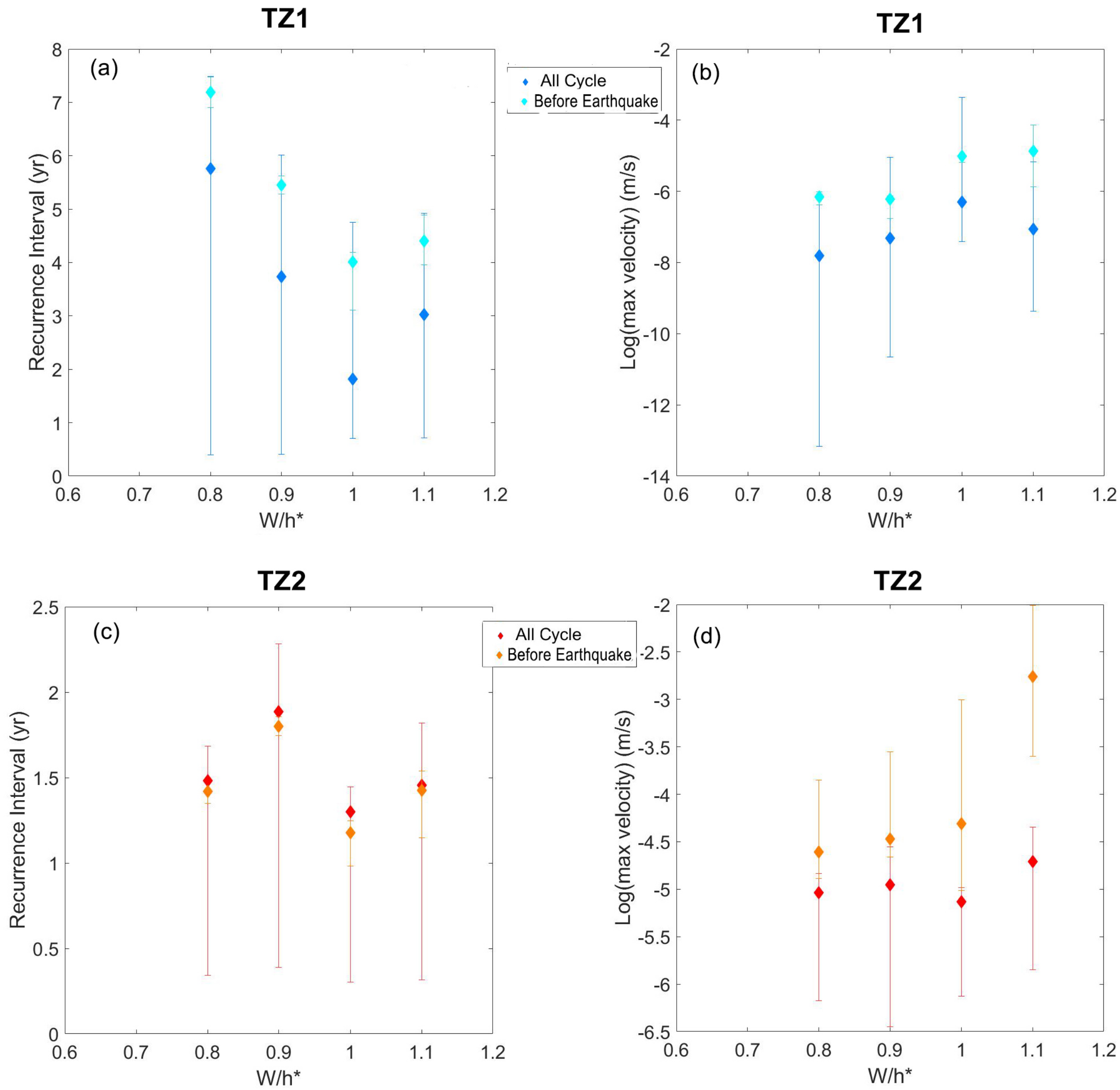

Figure 3.15: Graphs showing the recurrence interval and the maximum velocity in function of the W/h^* ratio for the transition zone 1 and the transition zone 2. We tested 4 cases : W/h^* = 0.80, W/h^* = 0.90, W/h^* = 1.0, W/h^* = 1.1. Diamonds represent the median value of the recurrence interval and maximum velocity with error bars. (a) and (b) are for TZ1, with results for the full cycle in blue, and for a few events in the $\sim$ 10 years before the megathrust earthquake in cyan. (c) and (d) are for TZ2, with the results for the full cycle in red, and for a few events in the $\sim$ 10 years preceding the megathrust earthquake in orange.

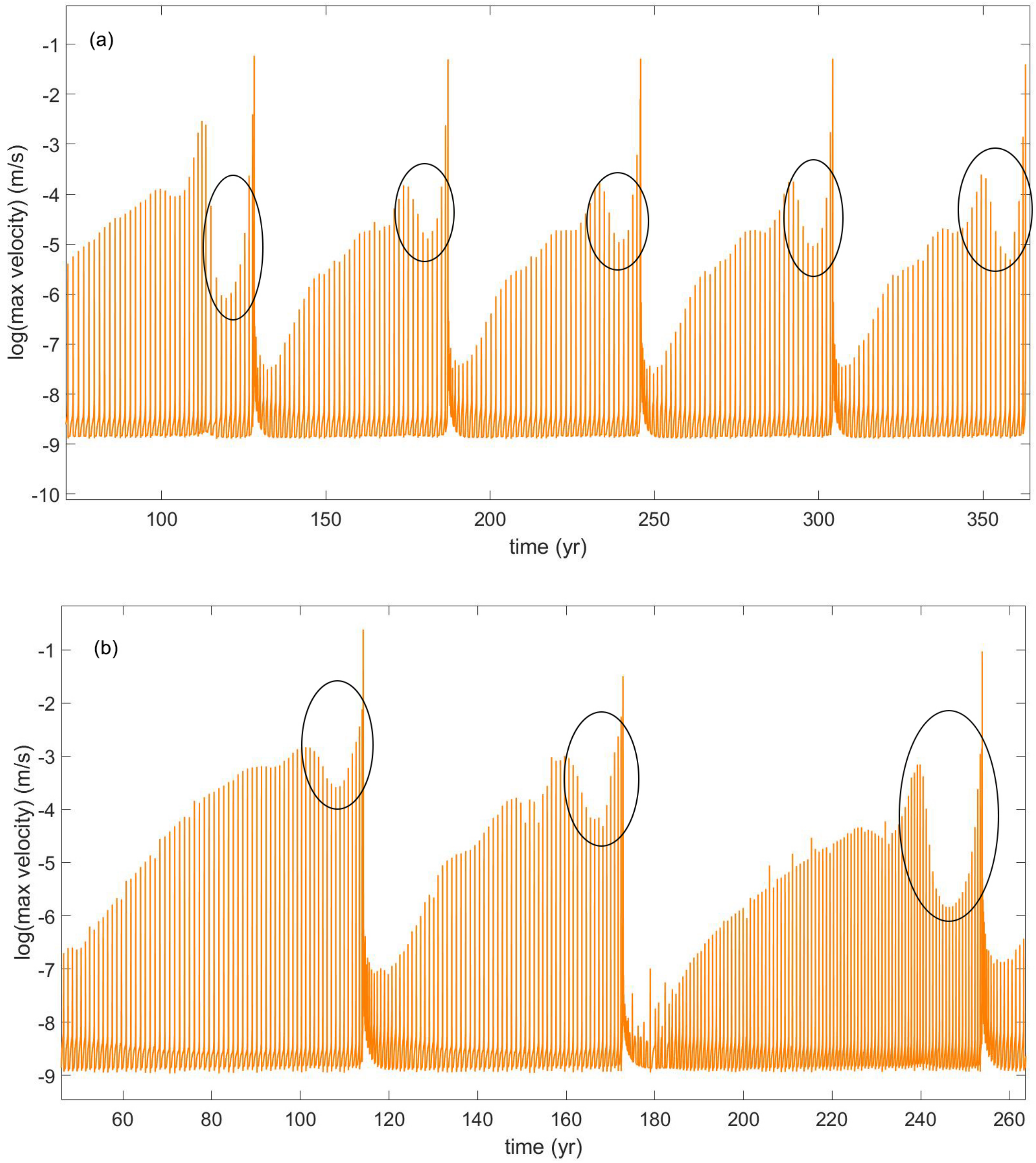

Figure 3.16: Maximum slip velocity versus time for (a) W/h^* = 0.8 (b) W/h^* = 1.1. Oval areas highlight the fluctuation in the SSE slip rate just before the earthquake.

maximum velocity before the earthquake is easily seen in the maximum velocity versus time plots but is not reflected in Figure 3.15. This is because we take the median of all maximum velocity for the full cycle, and the maximum velocity is lower ($\sim 10^{-7}$ m/s) at the beginning of the seismic cycle that during the pre-earthquake decrease ($\sim 10^{-5}$ m/s). For TZ1, we observe that the recurrence interval increases quite markedly in the years preceding the earthquake. For TZ2, the change reacts in the opposite way, with a slight decrease in the recurrence interval in the years preceding the earthquake. We calculate the error bar from the full 400-year seismic cycle by detecting all SSEs, and extracting the maximum and minimum interval found between two SSEs. This forms our error margin interval for the recurrence interval. The main point represented by the diamond is the median recurrence interval for all SSEs in the cycle. We follow the same procedure for the maximum velocity, extracting the maximum and minimum slip rates for all SSEs in the cycle and define it as our error margin interval.

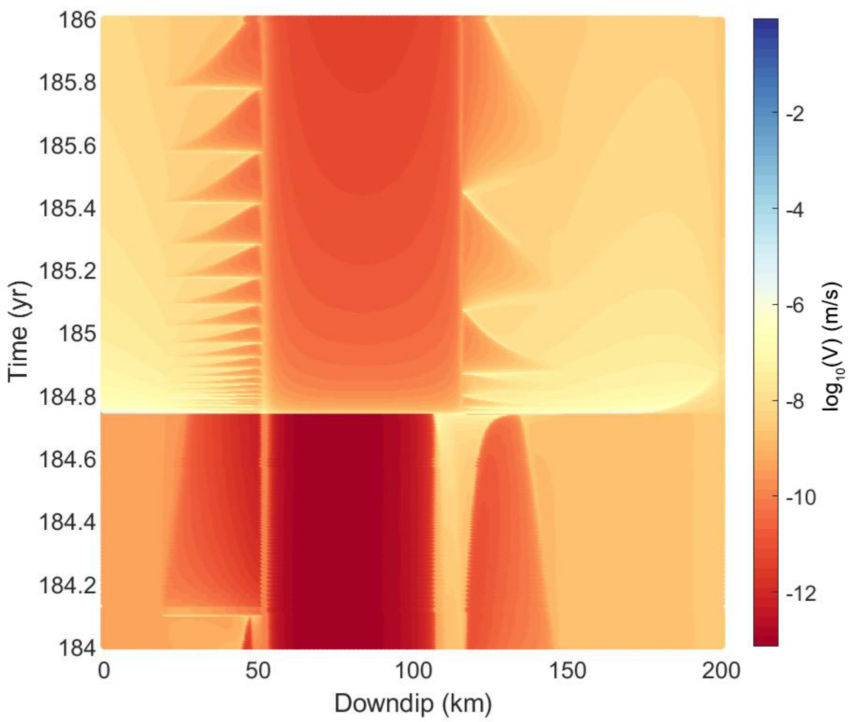

Figure 3.17: Snapshot of slip rate distribution of SSEs and megathrust earthquake, with x-axis being the downdip distance and y-axis being the time in years. Colorbar shows the logarithmic slip rate (m/s). At t=184.75 years, we can see the megathrust earthquake.

A snapshot of the slip rate distribution around megathrust nucleation (Figure 3.17) shows a change in the SSE patterns before and after the earthquake. It also shows a prolonged nucleation updip and downdip of the seismogenic zone just before the megathrust nucleation. After the event, we can see a succession of SSEs with a short recurrence interval before it stabilizes again. Location of shallow and deep SSEs before and after the megathrust earthquake are approximately the same.

3.4 Discussions and Conclusions

We used a 1D planar simulation in the framework of rate-and-state friction law to model the Costa Rica subduction zone. We created two velocity weakening zones, where SSEs can occur spontaneously. We then studied our results to find the optimal parameter sets that best reproduce the GPS observations of Costa Rica. Next, we studied the relationships between SSEs and earthquakes for transition zone 1 (above the seismogenic zone) and transition zone 2 (below the seismogenic zone).

Based on previous earthquake and aseismic slip modeling studies in the framework of rate-state friction, we chose model parameters ($\bar{\sigma}$ and L) by trial and error such that the outputs (recurrence interval and cumulative slip) are similar to the observations of earthquakes and slow slip events in the Costa Rica subduction zone. Specifically, the optimal parameter set is: $\bar{\sigma}$ = 35 MPa and L = 10 mm for the seismogenic zone to reproduce the 50-year earthquake cycle; to reproduce the $\sim$ 21 month SSE cycle, the optimal parameter set is: $\bar{\sigma}$ = 0.4 - 0.8 MPa for TZ1 and L = 0.2 - 0.5 mm; $\bar{\sigma}$ = 1.8 - 2.4 MPa and L = 0.5 - 0.8 mm TZ2. Our simulation seems to respect other observations from Costa Rica, such as slip, although our values (ranging between 2 cm and 5.5 cm) are in the low range, and duration (about 1.5 months).

We observed differences between shallow and deep SSEs in the recurrence interval for the same W/h^* ratio. Indeed, we obtain longer recurrence intervals for transition zone 1, even when we use lower values of $\bar{\sigma}$ and L than in transition zone 2. However, in the same transition zone, we manage to reduce the recurrence interval by using smaller values of $\bar{\sigma}$ and L. We propose two explanations for this phenomenon: (1) a difference in the values of $a - b$ between transition zone 1 and transition zone 2, which leads to different values of h^* and hence the ratio of the transition zone width to h^*, (2) a limitation of the code due to the fact that the shallow SSEs are really close to the beginning of the fault geometry, and the code may not be well stabilized yet.

Finally, just before an earthquake, we observe changes in recurrence intervals and maximum velocity. For TZ1, there is a large increase in both parameters in the 15 years before the earthquake. For TZ2, there is a small decrease in both maximum velocity and recurrence interval. This result is similar to the findings in a recent numerical study by Luo & Liu (2019), and could possibly help us to understand the observations of variable recurrence intervals of slow slip events prior to megathrust earthquakes in Guerrero, Mexico (Radiguet et al. 2016), and Boso, Japan (Hirose et al. 2012). A more systematic study is needed to quantify the variations in modeled shallow and deep SSEs source properties and their evoluation through an earthquake cycle.

4 Conclusions and Perspectives

4.1 Conclusion

Subduction zones generate the most devastating earthquakes and related hazards. In recent decades, scientists have discovered the presence of a specific type of slow earthquakes in subduction zones, called slow slip events (Dragert et al. 2001, Schwartz & DeShon 2007). Recently, many studies have focused on these SSEs, their mechanism and their relationship with earthquakes. Another important discovery was the fact that SSEs were detected in the transition zone above the seismogenic zone in some subduction zones (Voss et al. 2017), whereas the majority of SSEs had been discovered only downdip the seismogenic zone until now.

In this thesis, we focused on the relationship between updip and downdip SSEs, with each other, and with megathrust earthquakes in the Costa Rica subduction zone.

First, we worked with GPS inversion made on SSEs from Costa Rica to observe some parameters at the source and see how they scale with respect to earthquakes. Then, we worked on a numerical simulation in the rate-and-state framework to see under which conditions SSEs form in transition zones and how they can interact with earthquakes.

Our source parameters study in Chapter 2, highlight the fact that SSEs and earthquakes follow different scales of moment-duration and stress drop value. We found that SSEs stress drop range between 0.01-0.1 MPa, 1-2 order of magnitude smaller than earthquakes. These low values of stress drops can be explained by the fact that SSEs occur in near-lithostatic pore fluid pressure area because of metamorphic reactions (Audet et al. 2009), resulting in very low effective normal stress and limiting the level of shear stress on the fault, thus the stress drop. The duration-moment scale seems to follow the same linear trend that for SSEs calculated in other areas by Ide et al. (2007) and Gao et al. (2012), $\log M_0 \approx \log T$. It supports the idea that SSEs and earthquakes could be created from different mechanisms. However, we worked with few SSEs, and we would benefit from refining our study by adding more events. Also, it is possible that the moment-duration relation shows variation among individual margins, corresponding to the scaling $M_0 \propto T^n$ with the scaling factor n varying between 1 and 3 (Ide et al. 2007, Gao et al. 2012, Liu 2014, Michel et al. 2019). With more data of shallow SSEs, we would have been able to observe if shallow SSEs and deep SSEs are acting the same or are different. Most of our SSEs were located in the deep part of the slab, which does not allow a true analysis of shallow versus deep SSEs. To go further, and as the study of SSEs in Costa Rica intensifies, we can add new data to try to observe differences in the relationships between source parameters.

Our modeling studies the intrinsic SSE pattern changes as a function of different stages of the earthquake cycle. Our 1D model without along-strike variation allowed us to more effectively study the effects of different amplitudes, duration, loading functions, and starting times of disturbances. We observed that updip and downdip SSEs, even when they occur at approximately the same recurrence interval, do not propagate across the seismogenic zone. They also have different values of characteristic slip distance and effective normal stress due to the evolution of the friction parameter $a - b$, thus probably due to differences in the geology of the slab. Studies done by Xie et al. (2020) also indicates that shallow and deep SSEs do not have the same duration or magnitude. Recent numerical studies of SSEs have found that their behavior can change before a megathrust earthquake (Luo & Liu 2019). We were able to corroborate some of these observations with our own 1D simulation of Costa Rica. We observed that the updip and downdip SSEs do not follow the same evolution and change just before the megathrust. We found a small shortening of the SSE recurrence intervals and maximum slip velocities before the megathrust earthquake for deep SSEs, as well as an increasing of both recurrence intervals and maximum slip velocities in the years preceding the earthquake for shallow SSEs. The increasing reduction in the recurrence intervals and value of maximum SSE slip velocities just prior to a megathrust earthquake shows a continuous loading on the SSE regime with a progressive reduction in SSE size. These observations, if they can also be physically observed with GPS, may represent a distinctive earthquake preparation phase.

In our setup, shallow SSEs require lower values of L and $\bar{\sigma}$, due to the evolution of $a - b$. For this reason, we were able to simulate a recurrence interval of 20-22 months with a very low value of L = 0.3 mm. We reach the limits of the model and it is impossible to go below this value.

Finally, with improved GPS station coverage, the Costa Rica study has greatly improved, thus larger data sets and better offshore coverage will allow for more accurate observation of SSEs updip and downdip of the seismogenic zone, with better estimation of recurrence interval, maximum slip velocity, magnitude, and strain released. Thus, this will allow us to better constrain predictions of the magnitude of future megathrust ruptures.

4.2 Perspectives

4.2.1 3D Model

To go further and have a better understanding of the relationship between SSEs and megathrust earthquakes, we could work in 3D to incorporate realistic fault geometry, as various studies have shown that fault topographic features such as subducted seamounts an ridges could impact seismic rupture behaviour (Yang et al. 2013, Li & Liu 2016, Wang & Bilek 2011). Indeed, subduction geometry have long been suspected to control the modeled segmentation of SSEs and affect the source parameters of SSEs (Li & Liu 2016).The along-strike variation can affect the slip details of SSEs and megathrust earthquakes to certain extent. A quantitative investigation of the geometric effect has been conducted by Yang et al. (2013) using a 2D model, whose results indicate that when a seamount is close to an earthquake nucleation zone it could inhibit rupture propagation with either a higher or lower stength than the neighbouring segment. 3D simulations that account for along-strike variation and true geometric settings of the region of SSE and megathrust earthquakes are needed to better understand the relationship between megathrust earthquakes and SSEs if they are at different locations and distances.

In this regard, we have done preliminary work and found that the geometry of the Costa Rica subduction zone can be defined using the Slab2 geometric model (Hayes et al. 2018) which is an updated 3D model of global subduction zone geometries using a comprehensive set of geophysical observations. Thus, we created a triangular mesh to discretize this slab surface, and as we did for the 1D model, created two transition zones updip and downdip of the seismogenic zone with low values of effective normal stress and characteristic slip distance, where SSEs can occur spontaneously.

Taking into account both numerical accuracy and computational cost, we consider the 1 km grid as the optimal choice for our simulation. In total, we created 125,568 triangular elements in the non-planar fault model, which takes about two weeks to complete a 300-year sequence model.

From this preliminary result, we observed that, as it is the case for the 1D simulation, the shallow and deep SSEs do not occur with the same recurrence interval.

Moreover, we could extend the study outside the Nicoya Peninsula, to the whole subduction of Costa Rica, and thus work with different set of parameters for the three zones (southern, northern and central sections). Indeed, previous studies have shown that the roughness of the slab, as well as the depth of the transition zone is not the same along-strike (Outerbridge et al.

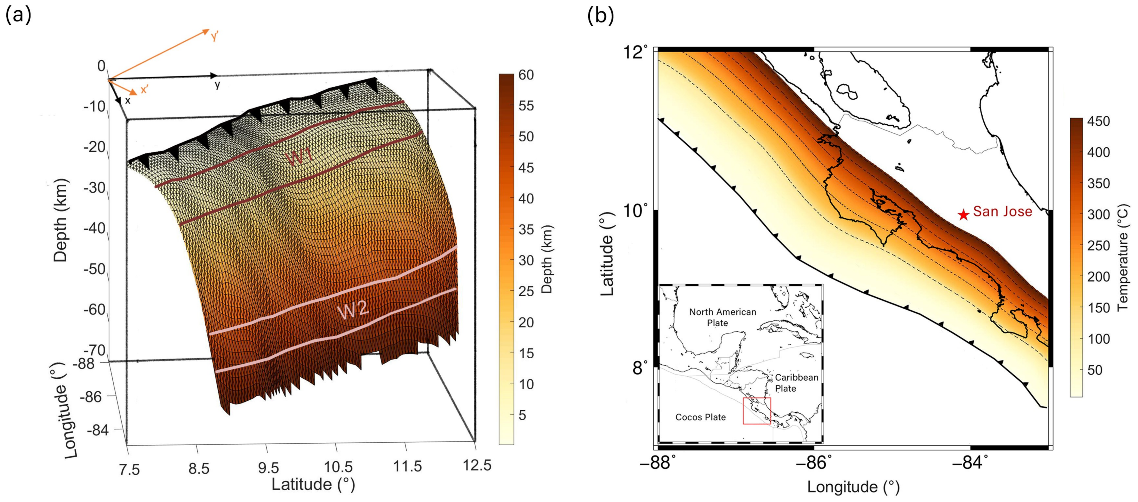

Figure 4.1: (a) 3-D nonplanar slab geometry for Costa Rica with triangular mesh of (element size is 5km for illustration purpose while spacing of 1km is used in simulations). Top orange cartesian coordinates X'-Y' is the rotation from the X-Y original coordinates. X' is trench-normal direction and Y' is trench-parallel direction.(b) Mapview of the temperature on the fault. Dash-dotted lines are depth contours every 10 km from 10 to 60 km depth.

2010). Under the Nicoya Peninsula, the updip transition zone varies from 5 to 14 km, and the downdip transition zone from 40 to 50 km; under the central region, the first transition zone is 5 to 10 km, while the second is shallower by 30 to 40 km; finally, under the Osa Peninsula, the up-dip transition zone is 5 to 10 km, and the down-dip zone is 35 to 45 km deep.

However, it is more difficult to compare numerical modeling with GPS observations in the other part of the Costa Rica subduction zones because very few SSEs have been recorded by GPS stations, as can be seen in the Table 1.1. However, with a well-defined model for the Nicoya Peninsula, it could be extended with a good estimate to the rest of the subduction zone of Costa Rica.

A 3D study would also allow us to more rigorously determine the magnitude of the SSEs, and to see if we observe a regular 21-month recurrence interval for events larger than 6.6 magnitude. In addition, a recent study (Xie et al. 2020) discovered that lower amounts of strain where released by shallow patches during earthquake and SSEs.

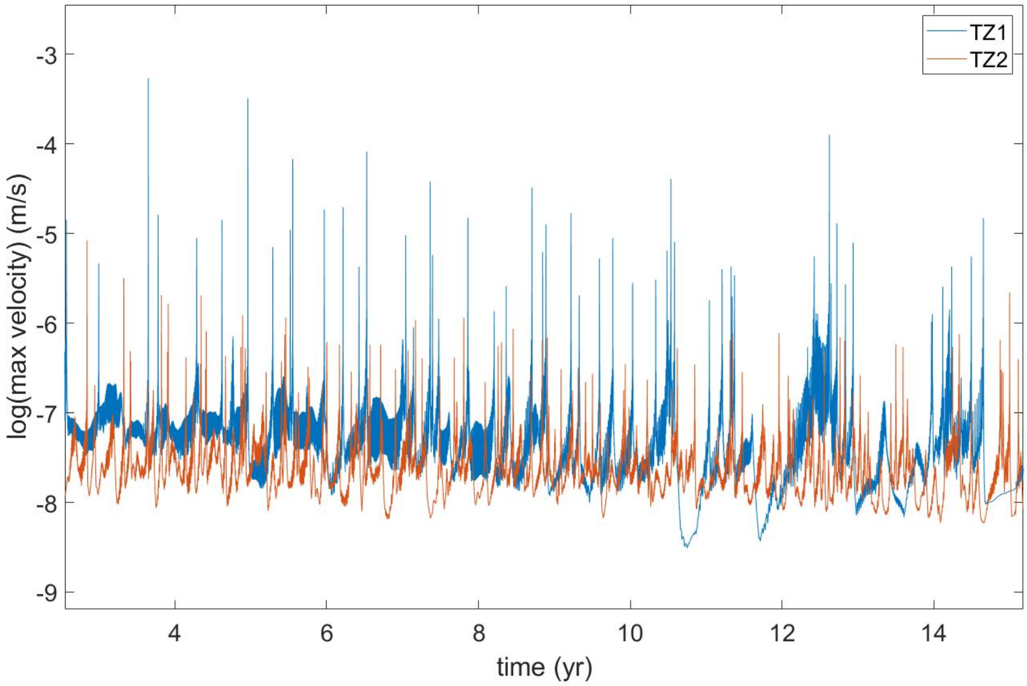

Figure 4.2: Comparison between transition zone 1 (shallow) and transition zone 2 (deep) in a preliminary 3D simulation for a short time period.

4.2.2 More Realistic 2D Model

Our study have shown variation in SSE behavior before and after a megathrust earthquake. This indicates that external tectonic processes can impact SSE patterns. However, it is still unclear if and how other external perturbations such as anthropogenic sources, volcanic eruptions, climatic factors, may affect the fault behavior and SSE pattern.

Also, the assumption of a uniform effective normal stress across the two transition zones, rather than a tapering distribution with depth may contribute to longer recurrence interval than realities. We could thus work on a new 2D model that incorporates an evolution of effective normal stress and characteristic slip distance inside the SSE areas.

We could also use a more complex 1D fault geometry with different dipping angles with depth. As the fault is not dipping the same all along the fault. Figure 4.3 show a possible evolution of the Costa Rica fault with depth for Nicoya Peninsula, using slip inversion (Norabuena et al. 2004).

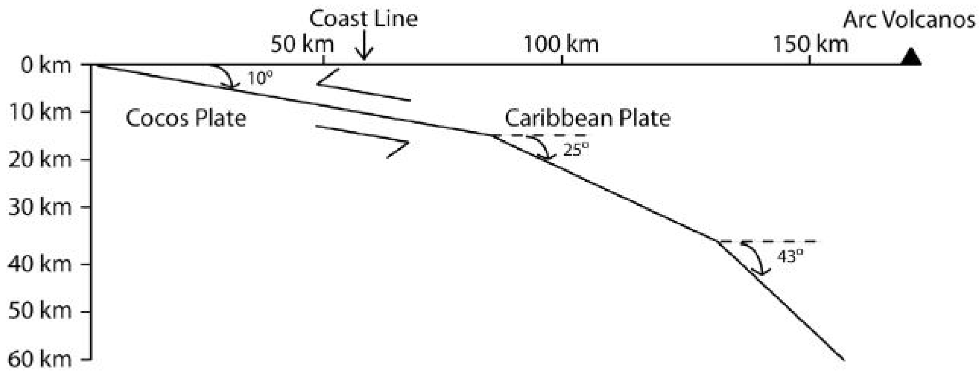

Figure 4.3: Fault geometry with different dipping angle in function of downdip distance (Norabuena et al. 2004). From the trench to 15 km depth, the interface dips at 10°; from 15 km to 38 km depth, the interface dips at 25°; and from 38 km to 60 km, the interface dips at 43°.

References

Aki, K. (1966), ‘Generation and propagation of g waves from the niigata earthquake of june 16, 1964.: Part 2. estimation of earthquake moment, released energy, and stress-strain drop from the g wave spectrum’, = *Bulletin of the Earthquake Research Institute, University of Tokyo* **44**(1), 73–88.

Allmann, B. P. & Shearer, P. M. (2009), ‘Global variations of stress drop for moderate to large earthquakes’, *Journal of Geophysical Research: Solid Earth* **114**(B1).

Ampuero, J.-P. & Rubin, A. M. (2008), ‘Earthquake nucleation on rate and state faults–aging and slip laws’, *Journal of Geophysical Research: Solid Earth* **113**(B1).

Arroyo, I. G., Husen, S. & Flueh, E. R. (2014), ‘The seismogenic zone in the central costa rican pacific margin: high-quality hypocentres from an amphibious network’, *International Journal of Earth Sciences* **103**(7), 1747–1764.

Audet, P., Bostock, M. G., Christensen, N. I. & Peacock, S. M. (2009), ‘Seismic evidence for overpressured subducted oceanic crust and megathrust fault sealing’, *Nature* **457**(7225), 76–78.

Audet, P. & Schaeffer, A. J. (2018), ‘Fluid pressure and shear zone development over the locked to slow slip region in cascadia’, *Science advances* **4**(3), eaar2982.

References

Barbot, S., Lapusta, N. & Avouac, J.-P. (2012), 'Under the hood of the earthquake machine: Toward predictive modeling of the seismic cycle', *Science* **336**(6082), 707–710.

Barckhausen, U., Ranero, C. R., von Huene, R., Cande, S. C. & Roeser, H. A. (2001), 'Revised tectonic boundaries in the cocos plate off costa rica: Implications for the segmentation of the convergent margin and for plate tectonic models', *Journal of Geophysical Research: Solid Earth* **106**(B9), 19207–19220.

Beeler, N., Tullis, T. & Weeks, J. (1994), 'The roles of time and displacement in the evolution effect in rock friction', *Geophysical Research Letters* **21**(18), 1987–1990.

Bhattacharya, P., Rubin, A. M., Bayart, E., Savage, H. M. & Marone, C. (2015), 'Critical evaluation of state evolution laws in rate and state friction: Fitting large velocity steps in simulated fault gouge with time-, slip-, and stress-dependent constitutive laws', *Journal of Geophysical Research: Solid Earth* **120**(9), 6365–6385.

Blanpied, M. L., Lockner, D. A. & Byerlee, J. D. (1995), 'Frictional slip of granite at hydrothermal conditions', *Journal of Geophysical Research: Solid Earth* **100**(B7), 13045–13064.

Blanpied, M., Marone, C., Lockner, D., Byerlee, J. & King, D. (1998), 'Quantitative measure of the variation in fault rheology due to fluid-rock interactions', *Journal of Geophysical Research: Solid Earth* **103**(B5), 9691–9712.

Day, S. M., Dalguer, L. A., Lapusta, N. & Liu, Y. (2005), 'Comparison of finite difference and boundary integral solutions to three-dimensional spontaneous rupture', *Journal of Geophysical Research: Solid Earth* **110**(B12).

DeMets, C. (2001), 'A new estimate for present-day cocos-caribbean plate motion: Implications for slip along the central american volcanic arc', *Geophysical research letters* **28**(21), 4043–4046.

References

DeShon, H. R., Schwartz, S. Y., Newman, A. V., González, V., Protti, M., Dorman, L. M., Dixon, T. H., Sampson, D. E. & Flueh, E. R. (2006), 'Seismogenic zone structure beneath the nicoya peninsula, costa rica, from three-dimensional local earthquake p-and s-wave tomography', *Geophysical Journal International* **164**(1), 109–124.

Dieterich, J. H. (1979), 'Modeling of rock friction: 1. experimental results and constitutive equations', *Journal of Geophysical Research: Solid Earth* **84**(B5), 2161–2168.

Dixon, T. H., Jiang, Y., Malservisi, R., McCaffrey, R., Voss, N., Protti, M. & Gonzalez, V. (2014), 'Earthquake and tsunami forecasts: Relation of slow slip events to subsequent earthquake rupture', *Proceedings of the National Academy of Sciences* **111**(48), 17039–17044.

Dragert, H., Wang, K. & James, T. S. (2001), 'A silent slip event on the deeper Cascadia subduction interface', *Science* **292**(5521), 1525–1528.

Feng, L., Newman, A. V., Protti, M., Gonzalez, V., Jiang, Y. & Dixon, T. H. (2012), 'Active deformation near the nicoya peninsula, northwestern costa rica, between 1996 and 2010: Interseismic megathrust coupling', *Journal of Geophysical Research: Solid Earth* **117**(B6).

Field, E. H., Biasi, G. P., Bird, P., Dawson, T. E., Felzer, K. R., Jackson, D. D., Johnson, K. M., Jordan, T. H., Madden, C., Michael, A. J. et al. (2015), 'Long-term time-dependent probabilities for the third uniform california earthquake rupture forecast (ucerf3)', *Bulletin of the Seismological Society of America* **105**(2A), 511–543.

Furumoto, M. & Nakanishi, I. (1983), 'Source times and scaling relations of large earthquakes', *Journal of Geophysical Research: Solid Earth* **88**(B3), 2191–2198.

Gao, H., Schmidt, D. A. & Weldon, R. J. (2012), 'Scaling relationships of source parameters for slow slip events', *Bulletin of the Seismological Society of America* **102**(1), 352–360.

References

Geller, R. J. (1976), ‘Scaling relations for earthquake source parameters and magnitudes’, *Bulletin of the Seismological Society of America* **66**(5), 1501–1523.

Graham, S., DeMets, C., Cabral-Cano, E., Kostoglodov, V., Rousset, B., Walpersdorf, A., Cotte, N., Lasserre, C., McCaffrey, R. & Salazar-Tlaczani, L. (2015), Slow slip history for the mexico subduction zone: 2005 through 2011, *in* ‘Geodynamics of the Latin American Pacific Margin’, Springer, pp. 3445–3465.

Hanks, T. C. & Kanamori, H. (1979), ‘A moment magnitude scale’, *Journal of Geophysical Research: Solid Earth* **84**(B5), 2348–2350.

Harris, R. N., Spinelli, G., Ranero, C. R., Grevemeyer, I., Villinger, H. & Barckhausen, U. (2010), ‘Thermal regime of the Costa Rican convergent margin: 2. thermal models of the shallow middle america subduction zone offshore costa rica’, *Geochemistry, Geophysics, Geosystems* **11**(12).

Hawthorne, J. & Rubin, A. (2013), ‘Laterally propagating slow slip events in a rate and state friction model with a velocity-weakening to velocity-strengthening transition’, *Journal of Geophysical Research: Solid Earth* **118**(7), 3785–3808.

Hayes, G. P., Moore, G. L., Portner, D. E., Hearne, M., Flamme, H., Furtney, M. & Smoczyk, G. M. (2018), ‘Slab2, a comprehensive subduction zone geometry model’, *Science* **362**(6410), 58–61.

He, C., Wang, Z. & Yao, W. (2007), ‘Frictional sliding of gabbro gouge under hydrothermal conditions’, *Tectonophysics* **445**(3-4), 353–362.

Hirose, H., Hirahara, K., Kimata, F., Fujii, N. & Miyazaki, S. (1999), ‘A slow thrust slip event following the two 1996 hyuganada earthquakes beneath the bungo channel, southwest japan’, *Geophysical Research Letters* **26**(21), 3237–3240.

References

Hirose, H., Kimura, H., Enescu, B. & Aoi, S. (2012), 'Recurrent slow slip event likely hastened by the 2011 tohoku earthquake', *Proceedings of the National Academy of Sciences* **109**(38), 15157–15161.

Hobbs, T., Kyriakopoulos, C., Newman, A., Protti, M. & Yao, D. (2017), 'Large and primarily updip afterslip following the 2012 mw 7.6 nicoya, costa rica, earthquake', *Journal of Geophysical Research: Solid Earth* **122**(7), 5712–5728.

Ide, S., Beroza, G. C., Shelly, D. R. & Uchide, T. (2007), 'A scaling law for slow earthquakes', *Nature* **447**(7140), 76–79.

Ishida, R., Hiramatsu, Y., Matsuzawa, T. & Obara, K. (2013), 'Average slip rate at the transition zone on the plate interface beneath the kii peninsula, japan, estimated from deep low-frequency tremors', *Earth, Planets and Space* **65**(9), 1047–1051.

Ito, Y., Hino, R., Kido, M., Fujimoto, H., Osada, Y., Inazu, D., Ohta, Y., Iinuma, T., Ohzono, M., Miura, S. et al. (2013), 'Episodic slow slip events in the japan subduction zone before the 2011 tohoku-oki earthquake', *Tectonophysics* **600**, 14–26.

Jiang, Y., Wdowinski, S., Dixon, T. H., Hackl, M., Protti, M. & Gonzalez, V. (2012), 'Slow slip events in costa rica detected by continuous gps observations, 2002–2011', *Geochemistry, Geophysics, Geosystems* **13**(4).

Kanamori, H. & Anderson, D. L. (1975), 'Theoretical basis of some empirical relations in seismology', *Bulletin of the seismological society of America* **65**(5), 1073–1095.

Kano, M., Kato, A., Ando, R. & Obara, K. (2018), 'Strength of tremor patches along deep transition zone of a megathrust', *Scientific reports* **8**(1), 1–8.

Kirkpatrick, J. D., Edwards, J. H., Verdecchia, A., Kluesner, J. W., Harrington, R. M. & Silver,

E. A. (2020), 'Subduction megathrust heterogeneity characterized from 3d seismic data', *Nature Geoscience* **13**(5), 369–374.

LaBonte, A. L., Brown, K. M. & Fialko, Y. (2009), 'Hydrologic detection and finite element modeling of a slow slip event in the costa rica prism toe', *Journal of Geophysical Research: Solid Earth* **114**(B4).

Lapusta, N. & Liu, Y. (2009), 'Three-dimensional boundary integral modeling of spontaneous earthquake sequences and aseismic slip', *Journal of Geophysical Research: Solid Earth* **114**(B9).

Lapusta, N. & Rice, J. R. (2003), 'Nucleation and early seismic propagation of small and large events in a crustal earthquake model', *Journal of Geophysical Research: Solid Earth* **108**(B4).

Lapusta, N., Rice, J. R., Ben-Zion, Y. & Zheng, G. (2000), 'Elastodynamic analysis for slow tectonic loading with spontaneous rupture episodes on faults with rate-and state-dependent friction', *Journal of Geophysical Research: Solid Earth* **105**(B10), 23765–23789.

Leeman, J., Saffer, D., Scuderi, M. & Marone, C. (2016), 'Laboratory observations of slow earthquakes and the spectrum of tectonic fault slip modes', *Nature communications* **7**(1), 1–6.

Li, D. & Liu, Y. (2016), 'Spatiotemporal evolution of slow slip events in a nonplanar fault model for northern Cascadia subduction zone', *Journal of Geophysical Research: Solid Earth* **121**(9), 6828–6845.

Linde, A. T., Gladwin, M. T., Johnston, M. J., Gwyther, R. L. & Bilham, R. G. (1996), 'A slow earthquake sequence on the san andreas fault', *Nature* **383**(6595), 65–68.

Liu, Y. (2014), 'Source scaling relations and along-strike segmentation of slow slip events in a 3-d subduction fault model', *Journal of Geophysical Research: Solid Earth* **119**(8), 6512–6533.

Liu, Y. & Rice, J. R. (2005), 'Aseismic slip transients emerge spontaneously in three-dimensional rate and state modeling of subduction earthquake sequences', *Journal of Geophysical Research: Solid Earth* **110**(B8).

Liu, Y. & Rice, J. R. (2007), 'Spontaneous and triggered aseismic deformation transients in a subduction fault model', *Journal of Geophysical Research: Solid Earth* **112**(B9).

Liu, Y. & Rice, J. R. (2009), 'Slow slip predictions based on granite and gabbro friction data compared to gps measurements in northern Cascadia', *Journal of Geophysical Research: Solid Earth* **114**(B9).

Liu, Y. & Rubin, A. M. (2010), 'Role of fault gouge dilatancy on aseismic deformation transients', *Journal of Geophysical Research: Solid Earth* **115**(B10).

Luo, Y. & Liu, Z. (2019), 'Slow-slip recurrent pattern changes: Perturbation responding and possible scenarios of precursor toward a megathrust earthquake', *Geochemistry, Geophysics, Geosystems* **20**(2), 852–871.

Marone, C. (1998), 'Laboratory-derived friction laws and their application to seismic faulting', *Annual Review of Earth and Planetary Sciences* **26**(1), 643–696.

Marone, C. J., Scholtz, C. & Bilham, R. (1991), 'On the mechanics of earthquake afterslip', *Journal of Geophysical Research: Solid Earth* **96**(B5), 8441–8452.

Michel, S., Gualandi, A. & Avouac, J.-P. (2019), 'Similar scaling laws for earthquakes and cascadia slow-slip events', *Nature* **574**(7779), 522–526.

References

Mouslopoulou, V., Bocchini, G. M., Cesca, S., Saltogianni, V., Bedford, J., Petersen, G., Gianniou, M. & Oncken, O. (2020), 'Earthquake swarms, slow slip and fault interactions at the western-end of the hellenic subduction system precede the mw 6.9 zakynthos earthquake, greece', *Geochemistry, Geophysics, Geosystems* **21**(12), e2020GC009243.

Norabuena, E., Dixon, T. H., Schwartz, S., DeShon, H., Newman, A., Protti, M., Gonzalez, V., Dorman, L., Flueh, E. R., Lundgren, P. et al. (2004), 'Geodetic and seismic constraints on some seismogenic zone processes in costa rica', *Journal of Geophysical Research: Solid Earth* **109**(B11).

Obara, K. (2002), 'Nonvolcanic deep tremor associated with subduction in southwest japan', *Science* **296**(5573), 1679–1681.

Obara, K., Hirose, H., Yamamizu, F. & Kasahara, K. (2004), 'Episodic slow slip events accompanied by non-volcanic tremors in southwest japan subduction zone', *Geophysical Research Letters* **31**(23).

Obara, K. & Kato, A. (2016), 'Connecting slow earthquakes to huge earthquakes', *Science* **353**(6296), 253–257.

Okada, Y. (1992), 'Internal deformation due to shear and tensile faults in a half-space', *Bulletin of the seismological society of America* **82**(2), 1018–1040.

Onwuemeka, J., Liu, Y. & Harrington, R. M. (2018), 'Earthquake stress drop in the charlevoix seismic zone, eastern canada', *Geophysical Research Letters* **45**(22), 12–226.

Outerbridge, K. C., Dixon, T. H., Schwartz, S. Y., Walter, J. I., Protti, M., Gonzalez, V., Biggs, J., Thorwart, M. & Rabbel, W. (2010), 'A tremor and slip event on the cocos-caribbean subduction zone as measured by a global positioning system (gps) and seismic network on the nicoya peninsula, costa rica', *Journal of Geophysical Research: Solid Earth* **115**(B10).

Ozawa, S. (2014), 'Shortening of recurrence interval of boso slow slip events in japan', *Geophysical Research Letters* **41**(8), 2762–2768.

Palmer, A. C. & Rice, J. R. (1973), 'The growth of slip surfaces in the progressive failure of over-consolidated clay', *Proceedings of the Royal Society of London. A. Mathematical and Physical Sciences* **332**(1591), 527–548.

Peng, Z., Vidale, J. E., Wech, A. G., Nadeau, R. M. & Creager, K. C. (2009), 'Remote triggering of tremor along the san andreas fault in central california', *Journal of Geophysical Research: Solid Earth* **114**(B7).

Perrin, G., Rice, J. R. & Zheng, G. (1995), 'Self-healing slip pulse on a frictional surface', *Journal of the Mechanics and Physics of Solids* **43**(9), 1461–1495.

Protti, M., Gu, F., McNally, K. et al. (1994), 'The geometry of the wadati-benioff zone under southern central america and its tectonic significance: Results from a high-resolution local seismographic network', *Physics of the Earth and Planetary Interiors* **84**(1-4), 271–287.

Radiguet, M., Perfettini, H., Cotte, N., Gualandi, A., Valette, B., Kostoglodov, V., ... & Campillo, M. (2016), 'Triggering of the 2014 m w 7.3 papanoa earthquake by a slow slip event in guerrero, mexico', *Nature Geoscience* **9**(11), 829.

Ranero, C. R., Villaseñor, A., Phipps Morgan, J. & Weinrebe, W. (2005), 'Relationship between bend-faulting at trenches and intermediate-depth seismicity', *Geochemistry, Geophysics, Geosystems* **6**(12).

Reber, J. E., Lavier, L. L. & Hayman, N. W. (2015), 'Experimental demonstration of a semi-brittle origin for crustal strain transients', *Nature Geoscience* **8**(9), 712–715.

Rice, J. R. (1993), 'Spatio-temporal complexity of slip on a fault', *Journal of Geophysical Research: Solid Earth* **98**(B6), 9885–9907.

Rogers, G. & Dragert, H. (2003), 'Episodic tremor and slip on the cascadia subduction zone: The chatter of silent slip', *Science* **300**(5627), 1942–1943.

Rolandone, F., Nocquet, J.-M., Mothes, P. A., Jarrin, P., Vallée, M., Cubas, N., Hernandez, S., Plain, M., Vaca, S. & Font, Y. (2018), 'Areas prone to slow slip events impede earthquake rupture propagation and promote afterslip', *Science advances* **4**(1), eaao6596.

Rousset, B., Bürgmann, R. & Campillo, M. (2019), 'Slow slip events in the roots of the san andreas fault', *Science advances* **5**(2), eaav3274.

Rubin, A. M. (2008), 'Episodic slow slip events and rate-and-state friction', *Journal of Geophysical Research: Solid Earth* **113**(B11).

Rubinstein, J. L., Vidale, J. E., Gomberg, J., Bodin, P., Creager, K. C. & Malone, S. D. (2007), 'Non-volcanic tremor driven by large transient shear stresses', *Nature* **448**(7153), 579–582.

Ruina, A. (1983), 'Slip instability and state variable friction laws', *Journal of Geophysical Research: Solid Earth* **88**(B12), 10359–10370.

Schwartz, S. & DeShon, H. (2007), 'Distinct updip limits to geodetic locking and microseismicity at the northern costa rica seismogenic zone: Evidence for two mechanical transitions', *The Seismogenic Zone of Subduction Thrust Faults* pp. 576–599.

Segall, P. & Bradley, A. M. (2012), 'Slow-slip evolves into megathrust earthquakes in 2d numerical simulations', *Geophysical Research Letters* **39**(18).

Segall, P., Desmarais, E. K., Shelly, D., Miklius, A. & Cervelli, P. (2006), 'Earthquakes triggered by silent slip events on kīlauea volcano, hawaii', *Nature* **442**(7098), 71–74.

Shelly, D. R. & Hardebeck, J. L. (2010), 'Precise tremor source locations and amplitude variations along the lower-crustal central san andreas fault', *Geophysical Research Letters* **37**(14).

References

Skarbek, R. M., Rempel, A. W. & Schmidt, D. A. (2012), 'Geologic heterogeneity can produce aseismic slip transients', *Geophysical Research Letters* **39**(21).

Socquet, A., Valdes, J. P., Jara, J., Cotton, F., Walpersdorf, A., Cotte, N., Specht, S., Ortega-Culaciati, F., Carrizo, D. & Norabuena, E. (2017), 'An 8 month slow slip event triggers progressive nucleation of the 2014 chile megathrust', *Geophysical Research Letters* **44**(9), 4046–4053.

Stuart, W. D. & Tullis, T. E. (1995), 'Fault model for preseismic deformation at parkfield, california', *Journal of Geophysical Research: Solid Earth* **100**(B12), 24079–24099.

Uchida, N., Iinuma, T., Nadeau, R. M., Bürgmann, R. & Hino, R. (2016), 'Periodic slow slip triggers megathrust zone earthquakes in northeastern japan', *Science* **351**(6272), 488–492.

Uchida, N., Matsuzawa, T., Ellsworth, W. L., Imanishi, K., Shimamura, K. & Hasegawa, A. (2012), 'Source parameters of microearthquakes on an interplate asperity off kamaishi, ne japan over two earthquake cycles', *Geophysical Journal International* **189**(2), 999–1014.

Voss, N., Dixon, T. H., Liu, Z., Malservisi, R., Protti, M. & Schwartz, S. (2018), 'Do slow slip events trigger large and great megathrust earthquakes?', *Science advances* **4**(10), eaat8472.

Voss, N. K., Malservisi, R., Dixon, T. H. & Protti, M. (2017), 'Slow slip events in the early part of the earthquake cycle', *Journal of Geophysical Research: Solid Earth* **122**(8), 6773–6786.

Wang, K. & Bilek, S. L. (2011), 'Do subducting seamounts generate or stop large earthquakes?', *Geology* **39**(9), 819–822.

Wei, M., Kaneko, Y., Shi, P. & Liu, Y. (2018), 'Numerical modeling of dynamically triggered shallow slow slip events in New Zealand by the 2016 mw 7.8 kaikoura earthquake', *Geophysical Research Letters* **45**(10), 4764–4772.

References

Xie, S., Dixon, T. H., Malservisi, R., Jiang, Y., Protti, M. & Muller, C. (2020), 'Slow slip and inter-transient locking on the nicoya megathrust in the late and early stages of an earthquake cycle', *Journal of Geophysical Research: Solid Earth* **125**(11), e2020JB020503.

Yamashita, T. & Schubnel, A. (2016), 'Slow slip generated by dehydration reaction coupled with slip-induced dilatancy and thermal pressurization', *Journal of Seismology* **20**(4), 1217–1234.

Yang, H., Liu, Y. & Lin, J. (2013), 'Geometrical effects of a subducted seamount on stopping megathrust ruptures', *Geophysical Research Letters* **40**(10), 2011–2016.

Yu H., Liu Y., Y. H. N. J. (2018), 'Modeling Earthquake sequences along the Manila subduction zone: Effects of three-dimensional fault geometry', *Tectonophysics* **733**, 73–84.

Yue, H., Lay, T., Schwartz, S. Y., Rivera, L., Protti, M., Dixon, T. H., Owen, S. & Newman, A. V. (2013), 'The 5 september 2012 nicoya, costa rica mw 7.6 earthquake rupture process from joint inversion of high-rate gps, strong-motion, and teleseismic p wave data and its relationship to adjacent plate boundary interface properties', *Journal of Geophysical Research: Solid Earth* **118**(10), 5453–5466.

Zhang, L., He, C., Liu, Y. & Lin, J. (2017), 'Frictional properties of the south china sea oceanic basalt and implications for strength of the manila subduction seismogenic zone', *Marine Geology* **394**, 16–29.